https://doi.org/10.5194/egusphere-2026-1557
Preprint. Discussion started: 27 March 2026

A Raster–Vector Framework for Multi-Scale Hydrological–Hydraulic Modeling Across Large Domains

Mohamed Amine Berkaoui[1], Mohamed Saadi[1], François Colleoni[2], Ngo Nghi Truyen Huynh[3], Ahmad Akhtari[3], Kevin Larnier[2], Hélène Roux[1], and Pierre-André Garambois[3]

[1]Univ Toulouse, Toulouse INP, CNRS, IMFT, Toulouse, France
[2]Hydro Matters, Toulouse, France
[3]INRAE RECOVER, Aix-Marseille Université, Aix-en-Provence, France

Correspondence: Mohamed Amine Berkaoui (amine.berkaoui@imft.fr)

Abstract. Hydrological models are widely used for large-scale flood modeling but typically rely on simplified routing schemes and a grid-based discretization that poorly capture river flow dynamics and geometry. Conversely, hydraulic models enable more accurate representation of flow dynamics through physically based routing schemes and vector-based geometry, but their application to large domains is constrained by significant parametrization challenges. Bridging these limitations requires integrated hydrological-hydraulic (H&H) modeling approaches capable of reconciling the spatial scale and structural mismatch between the two models while ensuring seamless coupling and computational efficiency for large-scale applications. We present an integrated raster-vector H&H modeling framework that leverages sub-grid representation of both river networks and drainage areas derived from high-resolution topography. The framework is implemented within the open-source `smash` modeling platform and integrates an end-to-end workflow from DEM preprocessing to internally coupled H&H simulations. The framework was evaluated over the Garonne river basin (France, 50 100 km^2) through one-directional coupling of a grid-based conceptual hydrological model with a vector-based 1D hydrodynamic model solving the zero-convective inertia approximation of the shallow water equations. Geometric preprocessing analysis performed across spatial resolutions ranging from 0.5 km to 10 km demonstrates that sub-grid information enable to maintain high spatial accuracy of DEM-derived sub-grid networks across scales in relation to the mapped hydrography, and reduces significantly catchment area errors compared to the default grid-based area delineation method. H&H simulations conducted at 1 km, 5 km, and 10 km without recalibration show robust preservation of flow timing across scales and demonstrate more stable streamflow bias across resolutions when using sub-grid drainage areas, while grid-based areas exhibit scale-dependent volume biases reflecting drainage area misrepresentation. The proposed H&H framework demonstrates scalable and efficient simulations at large domains within a unified modeling environment, offering promising perspectives for assimilation of multi-source water surface observations to infer key model parameters, addressing critical parametrization challenges in data-sparse regions.

1 Introduction

Flooding represents one of the most devastating natural hazards, causing significant loss of human life and economic damage worldwide. Flood modeling has emerged as an essential tool for predicting and managing these extreme events, enabling bet-

https://doi.org/10.5194/egusphere-2026-1557
Preprint. Discussion started: 27 March 2026

ter flood risk assessment and mitigation strategies. Hydrological models have been widely employed to assess flood hazards from local to global scales, with different levels of physical process representation, model structure, and spatial discretization (e.g. Clark et al. (2015)). In essence, a hydrological model partitions rainfall into runoff through vertical processes (such as infiltration, evapotranspiration, etc.) and then routes this runoff through the river network to the basin outlet. Despite their wide application for flood warning and management, hydrological models face two significant limitations. First, they typically employ simplified routing schemes (e.g., unit hydrographs, linear reservoirs, Muskingum method, kinematic wave) that may not adequately represent river flow dynamics, particularly in large and low-gradient basins (Li et al., 2021; Zhang et al., 2025). Second, most hydrological models are built on a Cartesian grid discretization due to their compatibility with widely available atmospheric and landscape gridded datasets (Lehner and Grill, 2013; Sood and Smakhtin, 2015). However, this grid-based structure inherently fails to capture fine-scale river features (e.g., sinuosity, length, drainage area) at coarser resolutions, while using finer resolutions leads to prohibitive computational costs (Mizukami et al., 2016). In contrast, hydraulic models implement more physically-based routing schemes by either solving full shallow water equations or an approximation neglecting convective inertia, enabling accurate representation of complex flow processes such as backwater effects. However, their application beyond the local scale faces significant parameterization challenges. Hydraulic models require inflow boundary conditions from gauge stations. However, these stations often have sparse spatial coverage, which limits the application of hydraulic models in poorly gauged or large basins (Chomba et al., 2021). Another major parameterization challenge concerns channel bathymetry, which characterizes river geometry (e.g., channel storage, thalweg elevation, bank slope), and is essential for accurate simulation of flood propagation and submersion (Dey et al., 2019). Detailed bathymetric data, typically requiring expensive and time-consuming field surveys, are rarely available at large scales, and despite bathymetric LiDAR's potential for larger coverage, its application remains limited to clear and shallow waters (Coppo Frias et al., 2025). Finally, hydraulic friction, which represents flow resistance and depends on local characteristics such as vegetation, cannot be measured directly and is typically calibrated as a uniform effective value per reach (Pappenberger et al., 2005). These parameterization challenges inevitably introduce uncertainties into hydraulic simulations, restricting their application to local scales and motivating the development of integrated modeling approaches.

The coupling of hydrological and hydraulic models (H&H) has emerged as an effective approach to compensate for their respective limitations, where a hydrological model provides physically consistent inflow conditions to be dynamically routed through the river network by a hydraulic model, allowing more accurate flow simulation at larger scales (Hoch et al., 2017; Zhang et al., 2025). The most common implementation is external coupling, a one-directional approach where the hydrological and hydraulic models run separately. In this approach, the outputs of the hydrological model (i.e. runoff) are processed offline and used to drive the hydraulic model. While straightforward to implement, this one-directional coupling approach requires separate model calibration missing parameter interactions (Zhang et al., 2025), and prevents information feedback between hydrological and hydraulic processes (e.g., floodplain infiltration, lateral seepage, open water evaporation; see Fleischmann et al. (2018); Dey et al. (2022)). In contrast, internal coupling provides an integrated framework where hydrological and hydraulic models exchange fluxes sequentially at their interfaces. This exchange can be one-directional (from hydrology to

https://doi.org/10.5194/egusphere-2026-1557
Preprint. Discussion started: 27 March 2026

hydraulics) or bidirectional when appropriate model structures are implemented, closing the loop between vertical hydrology and hydrodynamic processes.

A first critical challenge in H&H modeling lies in reconciling spatial scales between hydrological models operating on coarser grids and hydraulic models requiring fine-resolution vector-based river networks for accurate flood prediction, which is a local-scale process (Hoch et al., 2017). A common approach to address this type-scale mismatch is to aggregate coarse gridded runoff onto river network unit catchments through area-weighted mapping. This ensures mass conservation between hydrological grid cells and irregular catchment boundaries, as demonstrated in continental and global-scale flood modeling applications (Yamazaki et al., 2013; Li et al., 2022). However, this preprocessing step remains computationally intensive and presents ongoing efficiency challenges (Gharari et al., 2020; Li et al., 2022).

A second critical challenge in large-scale H&H modeling concerns the parameterization of the hydraulic model, particularly the representation of river channel bathymetry. Channel conveyance capacity (bankfull cross-sectional area) and thalweg elevation stand as the most essential bathymetric characteristics, critically influencing both fluvial hydrodynamics and surface-subsurface interactions in H&H models (Dey et al., 2022). In data-sparse large regions, H&H models typically assume simplified cross sectional shapes (e.g. rectangular), where bankfull width and depth are estimated through geomorphological relationships with drainage area or discharge, and thalweg elevation is subsequently derived from these estimated depths and digital elevation models (e.g., Paiva et al. 2011; Fleischmann et al. 2018). While practical, these simplified approaches introduce increased uncertainties, compromising the accuracy of flood simulations.

The growing availability of multi-source water surface observations, including satellite altimetry (e.g., SWOT, ICESat-2), airborne LiDAR and flood extent maps (e.g., GIEMS-2) offers a great opportunity to compensate for the scarcity of in-situ data and enhance flood modeling accuracy through data assimilation into H&H models.

H&H frameworks provide crucial hydrological closure (Larnier et al., 2025) to the ill-posed inverse problem encountered when assimilating water surface observations into stand-alone hydraulic models, where multiple parameter sets (i.e., inflows, bathymetry and friction) can produce similar water levels (Garambois and Monnier, 2015). By providing hydrologically consistent inflows across the basin, H&H approaches enable more physically coherent estimation of bathymetry and friction at the river network scale. Recent studies have demonstrated the potential of such integrated approaches by coupling hydrological models with hydraulic models and implementing variational data assimilation of multi-source observations. For instance, Larnier et al. (2025) coupled the semi-distributed MGB hydrological model (Pontes et al., 2017) with the DassFlow hydraulic model, which solves the full Saint-Venant equations and enables variational data assimilation of multi-source datasets. Such an approach is cornerstone to exploiting multi-source observations and performing information feedback to hydrological modules, as proposed in Pujol et al. (2022), and could be extended to recent learnable and regionalizable grid-based hydrological modeling and assimilation frameworks such as `smash` (Colleoni et al., 2025; Huynh et al., 2024, 2025, 2026), with the perspective of integrating hydraulic visibility from the SWOT satellite (Ledauphin et al., 2025) among other data sources and sensors.

In this context, it appears essential to develop scalable hydrological-hydrodynamic modeling approaches for large domains capable of efficiently assimilating multi-source observations. This raises a key methodological question: **What methodologi-**

https://doi.org/10.5194/egusphere-2026-1557
Preprint. Discussion started: 27 March 2026

cal framework and spatial structure should be adopted for a multi-scale, physically consistent hydrological–hydraulic modeling approach capable of efficiently assimilating multi-source data to infer key model parameters?

To address these challenges, we propose an integrated H&H modeling framework spanning the full chain from mesh generation to flood simulation in river channels. The framework's hybrid raster-vector structure reconciles the scale and structural mismatch between hydrological and hydraulic domains by combining coarse-grid distributed hydrology with fine-scale vector-based routing, enabling seamless and direct coupling between hillslope processes and channel dynamics. This unified modeling approach, integrated into the open source `smash` framework (source code: https://smash.recover.inrae.fr, documentation: https://github.com/DassHydro/smash), provides a flexible foundation for future data assimilation and optimization algorithms, paving the way for improved flood simulation at large scales.

The remaining sections of this paper are organized as follows. Section 2 presents the H&H modeling framework, including the coupling formulation, preprocessing workflow, and model implementation. Section 3 describes the study sites and datasets. Section 4 details the numerical experiment design, including model setup and evaluation strategy. Section 5 presents the results, Section 6 discusses the main findings, and Section 7 concludes the paper and outlines future research directions.

2 Methodology

In this section, we first present the general H&H modeling statement for coupling any grid-based hydrological model with a vector-based river network hydrodynamic model (Section 2.1). We then describe the preprocessing chain developed to implement the raster–vector coupling (Section 2.2), followed by the H&H modeling framework used for evaluation (Section 2.3).

2.1 Hydrological-hydraulic modeling one-directional coupling statement

The one-way coupled hydrological–hydraulic (H&H) model relies on the general principle of linking a distributed grid-based hydrological model $\mathcal{M}_{rr}$ with a vector-based river network hydraulic model $\mathcal{M}_{hy}$ such that:

$$\mathcal{M} = \mathcal{M}_{hy}\left(.\,;\,\mathcal{M}_{rr}(.)\right). \tag{1}$$

The two components are defined as follows:

- **Network hydraulics**: A hydraulic model $\mathcal{M}_{hy}$ is applied on the river network domain Ω_{hy}, composed of $s = 1..N_{seg}$ connected line segments, to simulate the spatio-temporal evolution of river wetted area A and discharge Q. It is forced by local runoff q_t and routed discharge Q_{rr} simulated by the gridded hydrological model, which determines upstream and lateral inflows, Q_{up} and Q_{lat}, such that:

$$\mathcal{M}_{hy} : (\cdot, Q_{up}, Q_{lat}) \;\mapsto\; (A, Q)(x,t), \qquad \forall x \in \Omega_{hy},\, t > 0 \tag{2}$$

- **Gridded hydrology**: Over the 2D basin grid Ω_{rr}, the hydrological model $\mathcal{M}_{rr}$ simulates runoff q_t from precipitation and evapotranspiration fields, P and E, and routes it to surface discharge Q_{rr} following the flow-direction map $\mathcal{D}_{\Omega_{rr}}$. Together with the coupling interface Γ_{rr-hy} defined during preprocessing, these fluxes provide the inflows to the hydraulic

https://doi.org/10.5194/egusphere-2026-1557
Preprint. Discussion started: 27 March 2026

model, such that:

$$\mathcal{M}_{rr} : (\cdot, P, E) \mapsto (q_t, Q_{rr}, Q_{up}, Q_{lat})(x', t), \qquad \forall x' \in \Omega_{rr},\, t > 0 \tag{3}$$

The coupling interface between the hydrological grid Ω_{rr} and the embedded vector-based hydraulic network Ω_{hy} is denoted Γ_{rr-hy}. It consists of N_{up} upstream and N_{lat} lateral inflow points defined by a mass-conservative hydrological–hydraulic coupling, which drains all cells of the upstream hydrological domain Ω_{rr} associated with the hydraulic network Ω_{hy} and its downstream outlet. This mapping is computed during the preprocessing step described hereafter.

2.2 Preprocessing chain for raster–vector coupling

The proposed preprocessing methodology breaks down into four major steps as summarized in Figure 1: (1) DEM conditioning through stream burning and depression filling; (2) flow direction computation at the DEM's native resolution followed by upscaling to target hydrological model resolution; (3) coarse-scale hydrography delineation by tracing reference vector river pathways along upscaled flow directions rather than using the conventional support area threshold approach; and (4) spatial coupling between the hydrological grid and the DEM-derived vector-based river network through direct cell-to-cell index matching. For the subsequent methodological steps, we use the open-source Python package `pyflwdir` (v0.5.10; https://github.com/Deltares/pyflwdir; Eilander 2022), which provides efficient methods for processing gridded topography, computing and upscaling flow directions for hydrological applications.

2.2.1 Step 1: Raw DEM conditioning

Raw DEMs often contain topographic depressions and flat areas, which hinder flow routing due to their undefined downslope directions. Depressions act as sinks producing disconnected flow paths and spurious sub-basins (Wang and Liu, 2006), while flat areas pose challenges for defining flow directions in low-relief areas where elevation data fails to capture crucial hydrologic features (e.g., narrow river valleys or multiple shallow drainage channels; see Lindsay (2016)). To address these challenges, we first apply the stream burning technique, which enforces mapped drainage patterns into the raw DEM, a conditioning process that has been applied in the production of the global hydrography datasets HydroSHEDS (Lehner et al., 2008; Lehner, 2022) and MERIT Hydro (Yamazaki et al., 2019). The vector-format reference hydrographic network is rasterized at the native DEM resolution and used as a binary mask to lower river cells elevation by a constant offset. We conducted a sensitivity analysis to evaluate the impact of the choice of the burning depth on the spatial alignment of DEM-derived networks with the reference hydrography, by testing depths from 0 to 100 m and using the Mean Separation Distance (MSD) as the evaluation metric (defined in Section 4.2). Results showed that most spatial accuracy improvements are achieved at moderate depths (20-40 m), with deeper burning yielding marginal gains but no degradation in network quality. Based on these results, we retained a burning depth of 100 m as a conservative choice to ensure complete removal of embedded historical channels. This choice only affects runoff routing computations and does not impact the topographic attributes for hydrodynamic modeling, which are retrieved from the unburned DEM (see Section 4.1.4). While stream burning enforces the alignment of flow paths with the reference river network, it does not resolve topographic depressions in hillslope cells. Therefore, a complementary conditioning

https://doi.org/10.5194/egusphere-2026-1557
Preprint. Discussion started: 27 March 2026

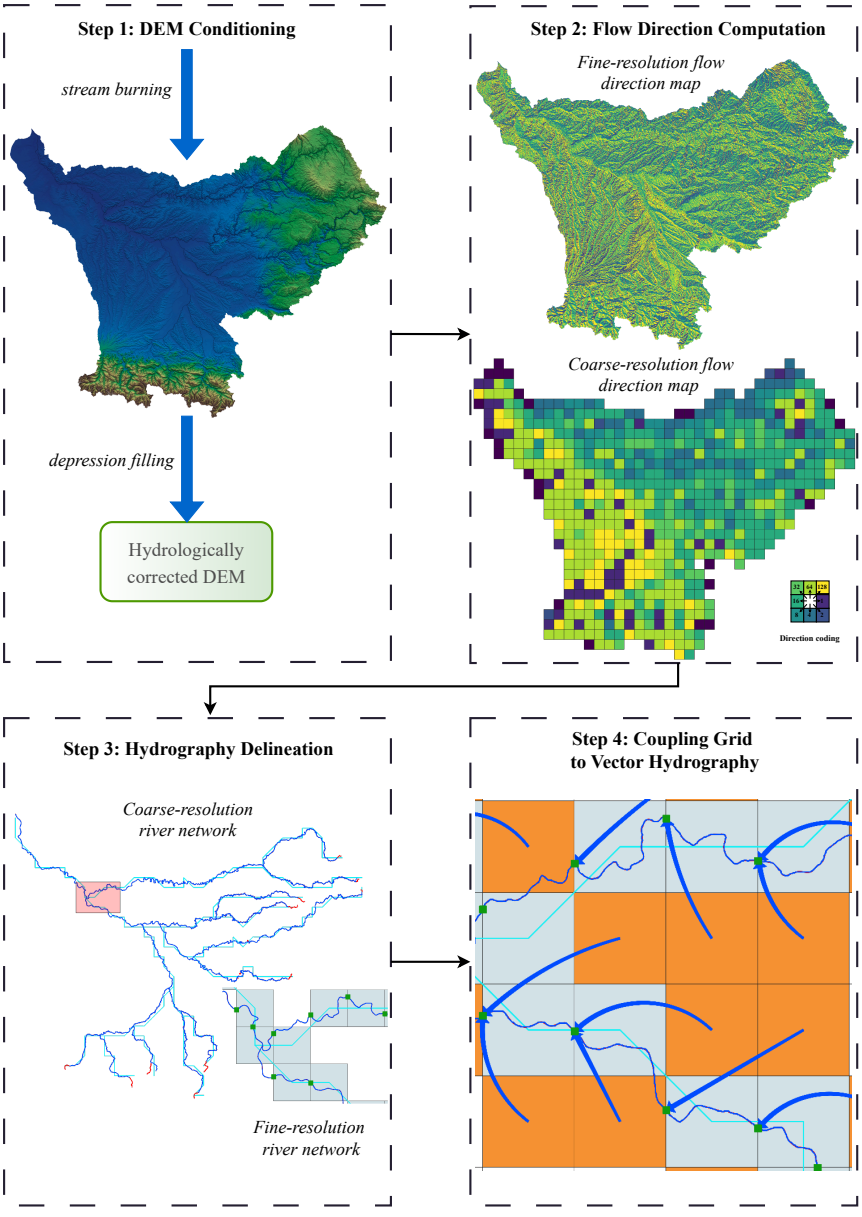

Figure 1. Overview of the preprocessing workflow for raster–vector coupling. **Step 1**: DEM conditioning through stream burning and depression filling. **Step 2**: Fine-resolution flow direction computation followed by upscaling to coarse hydrological model resolution. **Step 3**: Hydrography delineation producing both coarse-resolution river network (cyan) and sub-grid fine-resolution network (dark blue), with zoom-in view showing outlet pixels (green points) connecting coarse cells. **Step 4**: Spatial coupling between hydrological grid and vector-based river network, showing lateral inflows (orange cells) injecting gridded runoff into the sub-grid network through outlet pixels.

https://doi.org/10.5194/egusphere-2026-1557
Preprint. Discussion started: 27 March 2026

step is performed by filling topographic depressions using the algorithm of Wang and Liu (2006), which efficiently processes large-scale and high-resolution DEMs (Wang et al., 2019). The combined application of stream burning and depression filling produces a hydrologically corrected DEM with continuous flow paths preserving drainage connectivity while matching mapped river networks.

2.2.2 Step 2: Flow direction computation

The hydrologically corrected DEM produced in step 1 is used to compute the fine-resolution flow direction with the D8 algorithm (O'Callaghan and Mark, 1984), which routes water from each grid cell to one of its eight neighboring cells in the direction of the steepest downward slope. The D8 method remains the most widely used for hydrological modeling due to its deterministic non-dispersive nature, simple implementation, and computational efficiency with large raster datasets (Getirana et al., 2009; Kotyra and Chabudziński, 2023). This fine-resolution flow direction map is then upscaled to the target hydrological model resolution using the Iterative Hydrography Upscaling (IHU) algorithm (Eilander et al., 2021). The IHU method balances local information (i.e., from each cell and its eight neighbors) with global streams hierarchy to define the most representative sub-grid stream within each coarse-resolution cell, ensuring that upscaled flow directions accurately reflect the fine-scale hydrography. In practice, the algorithm identifies a representative river pixel in each coarse-resolution cell based on the largest upstream area within an effective area, an inner region to avoid selecting river segments that only pass through the cell's corners. From this pixel, the fine resolution flow path is traced downstream until the last pixel before exiting the coarse cell, which is designated as the outlet pixel. Coarse-resolution flow directions are then defined by connecting these outlet pixels following the fine-resolution flow paths between neighboring cells. IHU iteratively corrects erroneous coarse-resolution flow directions and optimizes the distance between connected outlet pixels. An illustration of the IHU upscaling concept is presented in Figure 2.

2.2.3 Step 3: hydrography delineation

The hydrography delineation process consists of two stages (see Figure 1, Step 3): first generating the coarse-resolution river network, and second deriving the corresponding fine-resolution river network using sub-grid data. In the first stage, a coarse river network is delineated by tracing stream paths from the reference vector hydrography along the upscaled flow direction map (produced in step 2). The conventional delineation approach consists of connecting grid cells with accumulated flow exceeding a specified threshold (i.e., critical support area). However, this threshold-based approach relies on an empirical and site-specific value, which varies with climatic and physiographic conditions, often leading to misalignments between modeled and reference river networks (McMaster, 2002; Vogt et al., 2003; Lin et al., 2021). As an alternative, we developed an algorithm that traces downstream river network paths along the upscaled flow direction map by evaluating, for each river segment of the reference network, nine candidate flow paths originating from the head cell and its eight neighboring cells. The path capturing the most number of segment vertices is then selected. The resulting paths are merged to form the complete coarse-resolution network. In the second stage, the fine-resolution river network is derived from the previously delineated coarse-resolution network by leveraging the seamless link between fine-scale and coarse-scale information preserved by the IHU upscaling algorithm (see Figure 2). For each coarse-resolution river cell, a sub-grid river channel is constructed by tracing the fine-resolution flow path

https://doi.org/10.5194/egusphere-2026-1557
Preprint. Discussion started: 27 March 2026

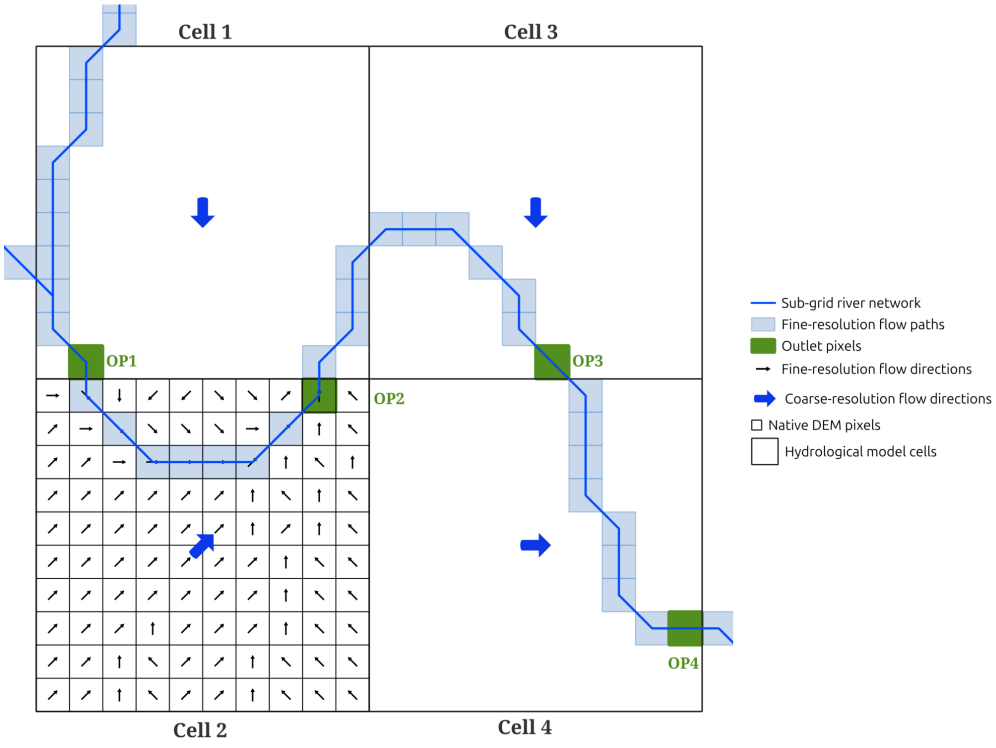

Figure 2. Procedure for determining coarse-resolution flow directions with the IHU method. From cell 1, the flow path is traced downstream from its outlet pixel (OP1) along the fine-resolution flow direction map until reaching the outlet pixel of a neighboring cell (OP2), thus assigning the coarse-resolution flow direction of cell 1 toward cell 2. Similarly, cell 2 flows toward cell 3 (OP2⟶OP3), and cell 3 flows toward cell 4 (OP3⟶OP4), following the fine-resolution flow paths between outlet pixels.

from its outlet pixel until reaching the outlet pixel of the next downstream coarse cell (see zoom-in view in Figure 1, Step 3). The resulting fine-resolution river network thus preserves the high spatial accuracy of the fine-resolution flow paths while following the connectivity defined by the coarse-scale river network topology. Note that the choice of the coarse resolution does not alter the fine-resolution flow paths. It only affects the derived fine-resolution river network by re-allocating outlet pixels according to the coarse grid cell boundaries.

2.2.4 Step 4: Spatial coupling of grid and vector-based hydrography

The final step of the workflow establishes the spatial coupling between the hydrological model grid and the derived sub-grid river network (see Figure 1, Step 4). Each coarse river cell is hydrologically connected to hillslope (non-river) cells through the coarse-resolution flow directions map, allowing gridded runoff to be routed from terrain cells into the sub-grid network through the outlet pixel of each river cell. Hillslope cell runoff is categorized into two types: (i) lateral inflows, which inject gridded runoff along the river network path (shown in orange in Figure 1, Step 4), and (ii) upstream inflows, which inject

https://doi.org/10.5194/egusphere-2026-1557
Preprint. Discussion started: 27 March 2026

gridded runoff at the upstream boundaries of river segments. This spatial coupling preserves distributed routing over the model grid while enabling vector-based in-channel river routing leveraging the fine-resolution sub-grid hydrography. The direct cell-to-cell index matching ensures explicit flux exchange from the grid to the vector domain, maintaining both mass balance and computational efficiency.

2.3 H&H modeling framework

2.3.1 `smash` platform

We implemented our hybrid raster-vector preprocessing algorithm within the `smash` (Spatially distributed Modeling and Assimilation for Hydrology) framework. `smash` is an open-source, differentiable and regionalizable modeling platform that enables modular high-resolution hydrological modeling and data assimilation from catchment to regional and country scales (Colleoni et al., 2025). The framework supports various vertical and lateral flow operators with spatially distributed routing schemes, enabling the simulation of discharge hydrographs and hydrological states across gridded domains. `smash` has been successfully deployed for both research applications (e.g., Colleoni et al. 2022; Huynh et al. 2023) and operational purposes, serving as the core solver of the French flash flood forecasting system (Piotte et al., 2020). In this work, we have extended `smash` by embedding a complete preprocessing chain tailored for hybrid raster-vector hydrological modeling, from DEM conditioning and fine-scale flow direction computation to upscaling and river network delineation. This fully integrated implementation enables seamless coupling between a gridded hydrological model and a vector-based river routing model within a unified modeling environment. The resulting hybrid configuration combines raster-based distributed runoff production and hillslope routing over the coarse-resolution grid with fine-scale vector-based in-channel river routing. Figure 3 provides an overview of the complete modeling chain. The following subsections detail the hydrological and hydrodynamic model components illustrated in Figure 3.

2.3.2 Hydrological model

Runoff production is simulated over basin grid cells using a spatially distributed implementation of the *GR4* conceptual model (Perrin et al., 2003; Mathevet, 2005), which transforms spatialized meteorological forcings (i.e., rainfall and potential evapotranspiration) into surface runoff through a reservoir-based approach. The *GR4* model comprises three storage components: (i) an interception reservoir with capacity c_i (mm) producing neutralized precipitation p_n (mm dt^{-1}) that feeds the production reservoir; (ii) a production reservoir with capacity c_p (mm) generating production runoff p_r and percolation p_{perc} (mm dt^{-1}); and (iii) a non-linear transfer reservoir with capacity c_t (mm) routing 90% of the generated runoff to produce the outflow q_r, while the remaining 10% is routed directly as q_d. A groundwater exchange flux, controlled by the parameter k_{exc} (mm dt^{-1}), acts on both routing components (q_r and q_d). The sum of both routing branches defines the total elemental discharge $q_t = q_d + q_r$ (mm dt^{-1}) produced at each hillslope grid cell.

https://doi.org/10.5194/egusphere-2026-1557
Preprint. Discussion started: 27 March 2026

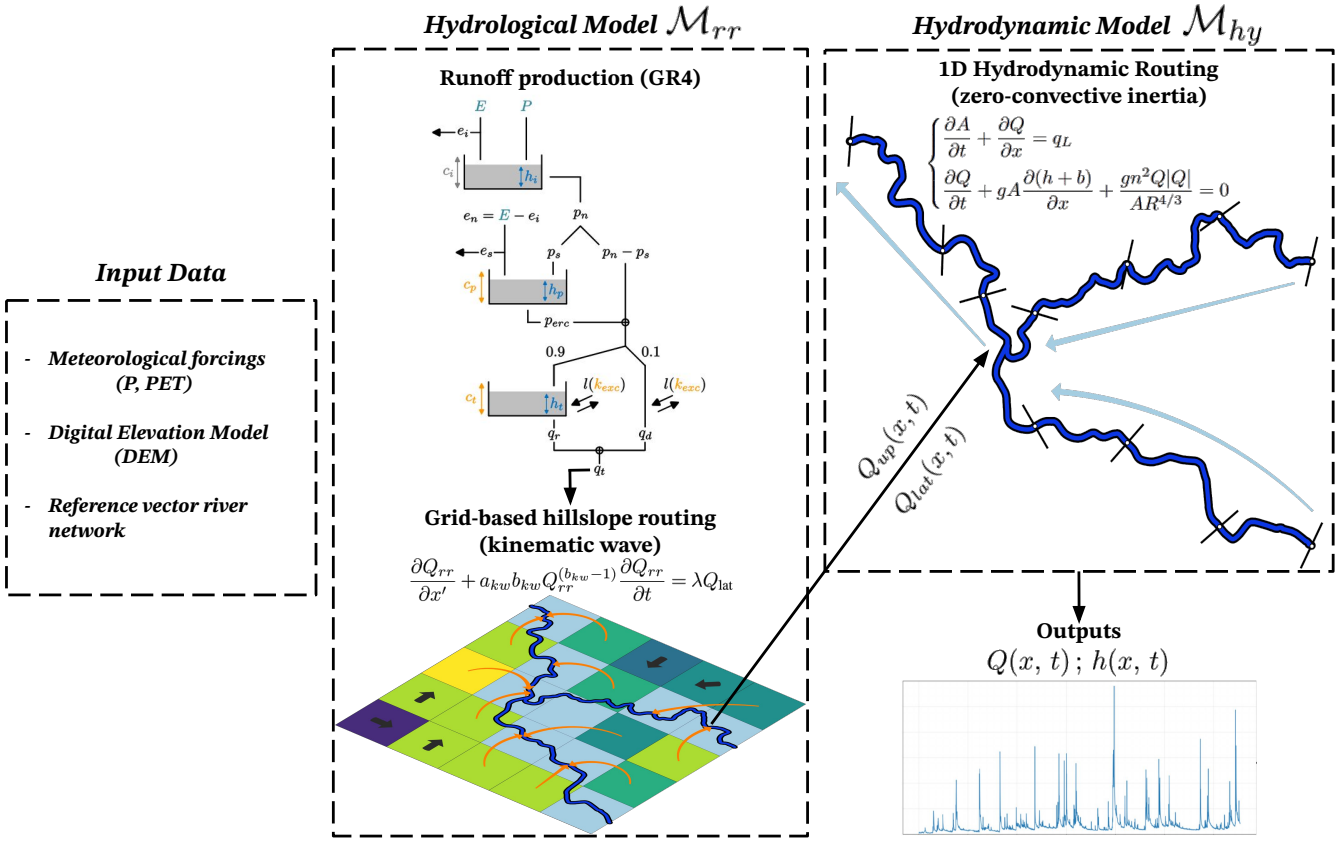

Figure 3. H&H modeling framework. Input data comprise meteorological forcings (precipitation P and potential evapotranspiration PET), Digital Elevation Model (DEM), and reference vector river network. DEM and river network are processed through the preprocessing workflow (Section 2.2) to generate the computational grid, sub-grid river network, cross-sections, and grid-vector coupling. The hydrological model ($\mathcal{M}_{rr}$) comprises runoff production (GR4) and grid-based hillslope routing (kinematic wave). Upstream and lateral hydrological inflows, $Q_{up}(x,t)$ and $Q_{lat}(x,t)$, are injected into the 1D hydrodynamic model ($\mathcal{M}_{hy}$) through the spatial coupling for in-channel routing using the zero-convective inertia approximation. Outputs include discharge $Q(x,t)$ and water depth $h(x,t)$ at computational cross-sections along the river network.

https://doi.org/10.5194/egusphere-2026-1557
Preprint. Discussion started: 27 March 2026

The elemental discharge q_t is subsequently routed over the hydrological hillslope grid cells following the flow direction map using a one-dimensional kinematic wave model discretized using a finite-difference scheme following (Chow et al., 1988):

$$\frac{\partial Q_{rr}}{\partial x'} + a_{kw} b_{kw} Q_{rr}^{(b_{kw}-1)} \frac{\partial Q_{rr}}{\partial t} = \lambda Q_{\text{lat}}, \qquad \forall x' \in \Omega_{rr}, t > 0 \tag{4}$$

where Q_{rr} denotes the discharge ("rr" refers to the routed discharge across the hydrological grid) and Q_{lat} ($\text{m}^3\,\text{s}^{-1}$) denotes the lateral inflow obtained by converting the elemental discharge q_t from runoff depth to volumetric discharge using the cell drainage area, λ is a unit conversion factor, and a_{kw} and b_{kw} are kinematic wave routing parameters. Spatially distributed hydrological parameters, $\boldsymbol{\theta}(x') = [c_i, c_p, c_t, k_{\text{exc}}, a_{kw}, b_{kw}]^T(x')$, governing both runoff production and lateral routing over hillslope grid cells, are estimated using a neural network-based regionalization approach (Huynh et al., 2024) (see Section 4.1.3). A key enhancement of this hybrid configuration lies in the propagation of sub-grid information into the hydrological model. Instead of using the nominal area of coarse-resolution grid cells (e.g., 1 km^2 for a 1 km resolution grid) for converting the elemental discharge q_t into lateral inflow Q_{lat}, we employ the actual sub-grid drainage area of each grid cell derived during the IHU upscaling process. This sub-grid drainage area is defined by the fine-resolution pixels draining to the outlet pixel of a grid cell and confined by upstream outlet pixels (Yamazaki et al., 2009; Eilander et al., 2021). By explicitly incorporating realistic drainage areas into the hydrological model, we mitigate the bias introduced by the oversimplification of natural boundaries inherent to regular grid discretization. This bias typically propagates from runoff production to streamflow simulation, often requiring unrealistic parameter values to compensate for discrepancies in drainage areas, thereby addressing the well-documented catchment-size problem associated with regular grid discretization at coarse resolutions (Shrestha et al., 2025).

2.3.3 Hydrodynamic model

For in-channel river routing, we employ a 1D hydrodynamic model based on the zero-convective inertia (also known as local inertial) approximation of the Saint-Venant equations (Bates et al., 2010). The zero-convective inertia 1D Saint-Venant system writes for a given river network segment:

$$\begin{cases} \dfrac{\partial A}{\partial t} + \dfrac{\partial Q}{\partial x} = q_L \\ \dfrac{\partial Q}{\partial t} + gA\dfrac{\partial (h+b)}{\partial x} + \dfrac{gn^2 Q|Q|}{AR^{4/3}} = 0 \end{cases}, \qquad \forall x \in \Omega_{hy}, t > 0 \tag{5}$$

where Q is the discharge ($\text{m}^3\ \text{s}^{-1}$), A is the cross-sectional area (m^2), h is the flow depth (m), b is the bed elevation (m), n is Manning's roughness coefficient ($\text{m}^{-1/3}$ s), R is the hydraulic radius (m), and g is gravitational acceleration ($\text{m}\ \text{s}^{-2}$), and q_L ($\text{m}^2\ \text{s}^{-1}$) represents the lateral inflow per unit length provided by the hydrological model, combining routed discharge Q_{rr} from hillslope grid cells and local runoff q_t generated over river grid cells (i.e., non routed discharge). The first equation represents mass conservation (continuity equation), explicitly coupling the hydraulic model to the hydrological model through the lateral inflow term q_L. The second equation represents momentum conservation, where only the advection term $\frac{\partial}{\partial x}\left(\frac{Q^2}{A}\right)$ of the full Saint-Venant momentum equation is neglected. This approximation is acceptable for large-scale natural rivers where flows are predominantly subcritical and vary gradually in space and time (Hunter et al., 2007; Neal et al., 2012; Yamazaki

https://doi.org/10.5194/egusphere-2026-1557
Preprint. Discussion started: 27 March 2026

et al., 2013), offering an interesting balance between realistic flow dynamics representation and computational efficiency for large-scale flood applications compared to simpler approximations and full shallow water equations. The hydrodynamic model is solved numerically using an explicit finite-difference scheme on a staggered grid, where the momentum and continuity equations are solved sequentially at each time step (Bates et al., 2010). In this discretization, discharge fluxes are computed at the interfaces between cross-sections, while water depths are evaluated at the centers of the cross-sections. Cross-sections correspond to outlet pixels of hydrological grid cells, forming a topologically connected dendritic network (sub-grid network). The complete numerical scheme is detailed in Appendix A.

3 Study sites and data

3.1 Garonne basin

The Garonne river basin, located in southwestern France, drains an area of about 56,000 km^2 and shows contrasted topographic and hydro-climatic conditions (see Figure 4). The Garonne river originates in the Spanish Pyrenees and flows for nearly 530 km before reaching the Atlantic Ocean through the Gironde estuary. The basin spans three major geographic entities: (i) the Pyrenees Mountains in the south, with high elevation exceeding locally 3000 m, marked by a nival regime from Pyrenean spring snow-melt; (ii) the Massif Central plateau in the northeast where elevation reaches 1900 m and is mainly influenced by pluvial hydrological regime; (iii) the alluvial plain between these two regions, with low altitudes not exceeding a few hundred meters, whose hydrological regime is influenced by precipitation from the Pyrenees and Massif Central mountains (Pardé, 1935; Biancamaria et al., 2019). The Garonne river and its main tributaries rising from the Pyrenees and Massif Central, form a complex hydrological system subject to various Oceanic, Mediterranean and Mountainous climatic conditions, resulting in marked seasonal variability alternating between high flows, extreme flood events (maximum record at Tonneins: up to 8000 m^3 s^{-1} in June 1875) and extreme low flows (lowest record: 37.5 m^3 s^{-1} in August 1989). For this study, the basin domain is limited to the Tonneins gauging station, draining an area of 50,100 km^2, as it's the most downstream point not influenced by the tidal effect of the estuary. Although the Garonne basin is highly anthropized with numerous dams and flood diversion channels (e.g., for navigation or agricultural irrigation), this study focuses exclusively on natural flow processes and therefore only the mapped natural river network is considered.

3.2 Data

3.2.1 Mapped river network

The reference hydrographic network is derived from BD TOPAGE®, the French national hydrographic reference dataset co-produced by the National Institute of Geographic Information (IGN) and the French Office for Biodiversity (OFB) (Sandre, 2020). BD TOPAGE® is a large-scale vector database providing the most exhaustive national hydrographic reference for France, derived from aerial imagery analysis and field survey validation, produced at a 1:5000 scale with 1 m spatial resolution. For this study, we retained only the main rivers of the Garonne basin and their major tributaries (see Figure 4). This

https://doi.org/10.5194/egusphere-2026-1557
Preprint. Discussion started: 27 March 2026

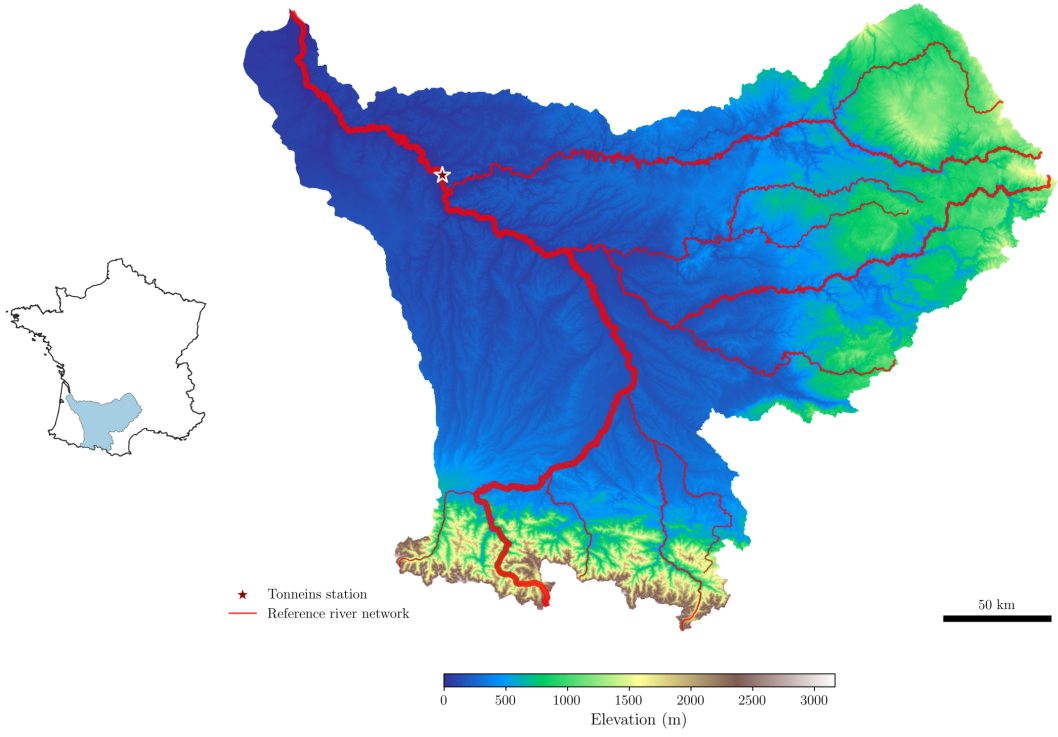

Figure 4. Study area of the Garonne river basin showing topography and reference hydrographic network (red lines with variable width representing discharge magnitude). The red star indicates the Tonneins gauging station marking the downstream limit of the study domain (50 100 km^2).

filtering ensures consistency between the mapped river network and the grid resolutions considered (up to 10 km), while pre-
290 serving realistic drainage patterns and avoiding stream collision artifacts that may arise when upscaling narrow, low-order streams, thereby achieving an optimal balance between hydrographic accuracy and computational efficiency for large-scale H&H modeling. The selected network comprises 11 river segments, with a total river length of ∼2680 km, ranging from ∼75 km to ∼530 km (Garonne river).

3.2.2 Digital Elevation Models (DEMs)

295 For topography data, we used two open source DEMs: the national BD ALTI® 25M DEM (IGN, 2017) and the global Multi-Error-Removed Improved-Terrain DEM (MERIT DEM) (Yamazaki et al., 2017). The BD ALTI® 25M is a national-scale DEM produced by IGN providing elevation data on a regular 25 m × 25 m grid generated from aerial photogrammetry, satellite imagery, and LiDAR surveys. The MERIT DEM was produced by removing major error components from existing spaceborne satellites (e.g., absolute bias and tree canopy bias), providing global coverage at 3 arc-second spatial resolution (∼90 m at the

https://doi.org/10.5194/egusphere-2026-1557
Preprint. Discussion started: 27 March 2026

equator). In order to ensure accurate multiplicity between native DEM resolutions and target resolutions, the MERIT DEM was resampled to a regular 100 m × 100 m grid using a bilinear interpolation.

3.2.3 Hydro-meteorological data

The hydrological model is forced with spatially distributed precipitation and potential evapotranspiration over the model grid. Hourly precipitation data are provided by the ANTILOPE J+1 product from Météo-France (Champeaux et al., 2009) at a resolution of 1 km × 1 km. Potential evapotranspiration is computed from SAFRAN temperature data (Quintana-Seguí et al., 2008; Vidal et al., 2010), originally at 8 km × 8 km resolution and downscaled to 1 km × 1 km, using the method of Oudin et al. (2005) producing interannual potential evapotranspiration. Observed discharge time series for model evaluation are obtained from the French national hydrometric database (Banque Hydro, https://hydro.eaufrance.fr).

4 Numerical experiment

4.1 Model setup

We adopt a spatially distributed model configuration using a state-of-the-art radar rainfall product, a high-resolution DEM, and a vector river network. Model parameters rely on a priori estimates derived from a previously calibrated hydrological model, complemented by hydraulic geometry and friction parameters obtained from standard empirical relationships. This setup is sufficient for evaluating the proposed modeling framework, as it provides realistic hydrological forcing and parameterization while allowing us to assess the internal consistency of the H&H framework and verify key numerical properties, particularly discharge performance, mass conservation, and computational efficiency.

4.1.1 Spatio-temporal configuration

The H&H modeling framework is evaluated at three computational spatial resolutions: 1 km, 5 km and 10 km, with the 1 km configuration serving as the baseline resolution for inter-scale analysis. The spatial resolution of the hydrological model is defined by the computational grid cell size at each resolution (e.g., 5 km × 5 km). In contrast, the hydrodynamic model, implemented on the sub-grid river network, has a variable spatial resolution defined by the flow distance Δx_i between consecutive cross-sections, corresponding to outlet pixels of hydrological grid cells. Consequently, the spatial distribution of hydraulic cross-sections is inherently controlled by the hydrological model resolution. Statistical distributions of flow distances for both DEMs across all resolutions are provided in Table C1 in Appendix C. Simulations span the period 2018–2019, with the year 2018 serving as a warm-up and 2019 retained for performance analysis. The hydrological model operates at an hourly time step, while the hydrodynamic model uses an adaptive time step controlled by the Courant-Friedrichs-Lewy (CFL) stability condition (Equation A6).

https://doi.org/10.5194/egusphere-2026-1557
Preprint. Discussion started: 27 March 2026

4.1.2 Aggregation of meteorological forcings

Hourly precipitation and daily potential evapotranspiration data are provided at a native resolution of 1 km (see Section 3.2.3). For simulations at 5 km and 10 km, meteorological forcings are spatially aggregated using a simple arithmetic mean to match the computational mesh resolution for both DEMs.

4.1.3 Hydrological model parameterization

The gridded hydrological parameters (c_i, c_p, c_t, k_{exc}, a_{kw} and b_{kw}; see Section 2.3.2) are derived from a learnable regionalization approach with multi-gauge calibration (Huynh et al., 2024), applied to the Garonne basin at 1 km spatial resolution using a raster-based hydrological model configuration, without the vector-based routing framework introduced in the present work. This procedure, applied with semi-uniform constraints by sub-basins associated with the calibration gauges, produces "semi-distributed parameter fields" for the distributed model. The parameters for the models at 5 km and 10 km resolutions are derived by upscaling the 1 km baseline fields using arithmetic mean aggregation within each coarsened cell, without any further recalibration. Spatial distributions of hydrological parameters at each resolution are presented in Appendix B for both DEMs (Figures B1 and B2).

4.1.4 Hydraulic model parameterization

For the sub-grid network parameterization, cross-sections are assumed rectangular with bankfull width w_i and depth h_i estimated through geomorphological relationships with drainage area $A_{d,i}$ calibrated using hydraulic attributes of the French theoretical hydrographical network (RHT) (Pella et al., 2012):

$$w_i = 2A_{d,i}^{0.4}, \quad h_i = 0.15A_{d,i}^{0.24} \tag{6}$$

The drainage areas $A_{d,i}$ used in these geomorphological relationships are derived from fine-resolution flow directions (i.e., sub-grid drainage areas), ensuring more scale-consistent hydraulic geometry across computational resolutions. It is important to note that these geomorphological equations are derived from median reach-scale width and depth attributes available in the RHT, rather than bankfull conditions. This simplified parameterization provides a practical and spatially consistent representation of channel geometry at the scale of the Garonne basin, given the scarcity of observations of bankfull channel geometry across the river network. Channel bed elevation b_i is estimated by subtracting the geomorphological channel depth h_i from a hydrologically adjusted elevation using Yamazaki et al. (2012) method, which ensures a monotonic decrease in elevation from upstream to downstream cross-sections along the sub-grid drainage network and thus producing smooth longitudinal elevation profiles required for slope and flow calculations. Manning's roughness coefficient is set uniformly to $n = 0.05$. Spatial distributions of the hydraulic parameters along sub-grid network (w_i, h_i, b_i) across spatial resolutions are presented in Appendix C for both BDALTI and MERIT DEMs (Figures C1 and C2). In addition, an illustration of the hydrological elevation adjustment along the Garonne river with MERIT DEM is shown in Appendix C (Figure C3).

https://doi.org/10.5194/egusphere-2026-1557
Preprint. Discussion started: 27 March 2026

4.2 Quality assessment

4.2.1 Geometric assessment of the preprocessing

The geometric quality assessment is conducted across spatial resolutions ranging from 0.5 km to 10 km, including a finer resolution than those used in the H&H simulations (Section 4.1.1).

Visual inspection

The quality of both coarse-scale and sub-grid river networks is assessed qualitatively through visual comparison by overlaying the derived networks (coarse and sub-grid) with the reference hydrography across scales to inspect their spatial agreement. For visual clarity and to highlight the contrast between river networks retrieved at the fine and coarse resolutions, only the 1 km and 10 km scales are presented for this qualitative visual assessment.

Quantitative metrics

Quantitatively, we assessed network quality using two metrics to evaluate their spatial alignment and coverage with respect to the reference hydrography. To quantify the level of spatial displacement between the derived and reference networks, we computed the mean separation distance (MSD), defined as the average distance between each vertex of the reference network and its projection onto the derived network (Davies and Bell, 2009). Lower MSD values indicate better spatial alignment. To assess network completeness, we computed the Percentage Within Buffer (PWB) metric by quantifying the percentage of the reference network captured within a uniform buffer placed around the derived network (e.g., McMaster 2002), with lower values suggesting greater omission of mapped streams. The PWB metric is applied only to sub-grid networks using fixed buffer sizes of 25 m and 100 m for BDALTI- and MERIT-derived networks, corresponding to their native resolutions, respectively. This approach ensures consistent buffer sizing across scales and overcomes the scale-dependent limitation reported in previous studies, where buffer width varies with resolution when evaluating coarse river networks (e.g., Davies and Bell 2009; Sousa and Paz 2017; Almeida et al. 2024).

Catchment delineation accuracy

The impact of using drainage areas computed from fine-resolution flow directions in the hydrological model is assessed across all scales and for both DEMs by quantifying catchment delineation accuracy for both grid-based and sub-grid methods at 44 gauge stations distributed across the Garonne basin, spanning catchment sizes from 94 to 50,100 km^2 (median: $\sim$2,600 km^2; mean: $\sim$6,500 km^2). Gauge stations were allocated to outlet pixels (i.e., computational cross sections) using a weighted score minimizing area error and distance to station. At each station, the relative error in delineated catchment area is computed for both methods with respect to the reference station drainage area.

https://doi.org/10.5194/egusphere-2026-1557
Preprint. Discussion started: 27 March 2026

4.2.2 H&H model assessment

Performance metrics

The performance of the hydrological–hydraulic (H&H) simulations is assessed by comparing simulated discharge Q produced by the hydrodynamic model (Equation 5) with observed discharge Q^* at gauging stations using the modified Kling–Gupta Efficiency (KGE′; Kling et al. (2012)), defined as:

$$\mathrm{KGE}'(Q^*, Q) = 1 - \sqrt{(r-1)^2 + (\beta-1)^2 + (\gamma-1)^2}, \tag{7}$$

where r is the Pearson correlation coefficient between simulated and observed discharges, β is the bias ratio, and γ is the variability ratio defined as:

$$\beta = \frac{\mu}{\mu^*}, \qquad \gamma = \frac{\mathrm{CV}}{\mathrm{CV}^*} = \frac{\sigma/\mu}{\sigma^*/\mu^*}, \tag{8}$$

with CV the coefficient of variation, and μ and σ denoting the mean and standard deviation of simulated (Q) and observed (Q^*) discharges, respectively. The key distinction from the original KGE (Gupta et al., 2009) lies in the definition of the variability component. While the original KGE expresses variability using the standard deviation ratio $\alpha = \sigma_\mathrm{s}/\sigma_\mathrm{o}$, KGE′ instead uses the coefficient of variation ratio γ, which de-correlates bias and variability terms and thereby limits compensating effects between these components. All performance metrics are computed using the `hydroeval` Python package (Hallouin, 2021). To ensure robust performance assessment, only stations with complete discharge observations over the entire simulation period (2018–2019) are retained, reducing the dataset from 44 to 18 stations.

Finally, to assess the sensitivity of model performance and its computational efficiency to the CFL condition, we tested different sets of α_{CFL} values:

- 1 km: α_{CFL} = [0.9, 0.7] (restricted range for computational efficiency)
- 5 km: α_{CFL} = [0.9, 0.7, 0.5, 0.2]
- 10 km: α_{CFL} = [0.9, 0.7, 0.5, 0.2]

For each configuration (DEM, spatial scale, area delineation method), $\alpha_{CFL} = 0.9$ is used as the baseline. Lower α_{CFL} values (0.7, 0.5, 0.2) are selected only if they provide an improvement greater than 1% in the median KGE′ compared to the current best α_{CFL} value.

Mass balance conservation

The mass balance conservation between the hydrological basin domain Ω_{rr} and the river network hydraulic domain Ω_{hy} is evaluated by computing the mass balance error at each hydrological time step following Bates and De Roo (2000):

$$E_t = \frac{(V_{in,t} - V_{out,t}) - (V_{t+1} - V_t)}{V_{t+1}} \times 100 \tag{9}$$

https://doi.org/10.5194/egusphere-2026-1557
Preprint. Discussion started: 27 March 2026

where $V_{in,t}$ is the total volume of water entering the Ω_{hy} domain from upstream and lateral inflows during time step t [m^3], $V_{out,t}$ is the total volume leaving the Ω_{hy} domain at its downstream boundary (basin outlet) during time step t [m^3], V_t is the total volume of water stored in the Ω_{hy} domain at the beginning of time step t [m^3], and V_{t+1} is the total volume of water stored in the Ω_{hy} domain at the end of time step t [m^3]. The ideal value of E_t is 0%, indicating perfect mass conservation.

5 Results

5.1 Quality assessment of DEM-derived networks across scales

For visual clarity and to highlight the contrasted river networks retrieved at the fine and coarse resolutions, only the 1 km and 10 km scales are shown in Figure 5. Visual comparison of the derived networks at these resolutions for both DEMs at the chosen optimal burning depth (i.e., 100 m) shows that coarse networks fail to preserve the structure and spatial patterns of the reference network as resolution is coarsened, while sub-grid networks consistently maintain close spatial alignment, with some localized discrepancies that are further analyzed below. This visual inspection is further supported by the quantitative analysis in Figure 6, which shows that MSD increases substantially as the grid is coarsened, rising from around 90 m at 0.5 km resolution to nearly 2000 m at 10 km resolution, with both DEMs exhibiting a similar spatial accuracy degradation pattern for coarse river networks. In contrast, sub-grid networks perform much better, reducing MSD values by 66–95% and 69–83% compared to coarse networks for BDALTI and MERIT respectively. At 0.5 km and 1 km resolutions, sub-grid MSDs are consistently very low (6–10 m for BDALTI, 30–32 m for MERIT), before increasing sharply at 5 km and 10 km resolutions (200–660 m), though still remaining well below coarse network MSDs (Figure 6a). Sub-grid network completeness, assessed through the PWB metric, remains very high across scales, exceeding 99% at fine grid resolutions (0.5–1 km) and gradually decreasing to ∼95% for BDALTI and ∼94% for MERIT at 10 km resolution (Figure 6b). This decrease in completeness at coarser resolutions is directly linked to reference network omissions. Figure 6c shows that omissions in BDALTI sub-grid networks occur exclusively in headwater regions (up to ∼5% at 10 km), while MERIT sub-grid networks exhibit both headwater omissions (up to ∼5% at 10 km) and internal omissions (∼1%). When these omitted features are excluded from the analysis, MSD stabilizes at very low values (∼5 m for BDALTI and ∼25 m for MERIT) across all scales (Figure 6d).

5.2 Catchment size errors across delineation methods

We evaluated the effect of propagating actual drainage boundaries from fine-resolution flow directions into the hydrological mesh (sub-grid method) by comparing relative errors in catchment area at 44 gauge stations against the default coarse-resolution square grid cell (grid-based method). Figure 7 presents boxplots of relative catchment area errors for both BDALTI and MERIT DEMs across scales. The sub-grid method maintains high accuracy with absolute median relative errors consistently below 1% and mean absolute relative errors around 2% across all scales and both DEMs, with 56% of stations falling within ±1% relative area error. In contrast, the grid-based method shows greater variability particularly at coarser scales, with median and mean relative errors reaching up to 16% and 22% respectively for MERIT DEM at 10 km resolution, and only 28% within the ±1%

https://doi.org/10.5194/egusphere-2026-1557
Preprint. Discussion started: 27 March 2026

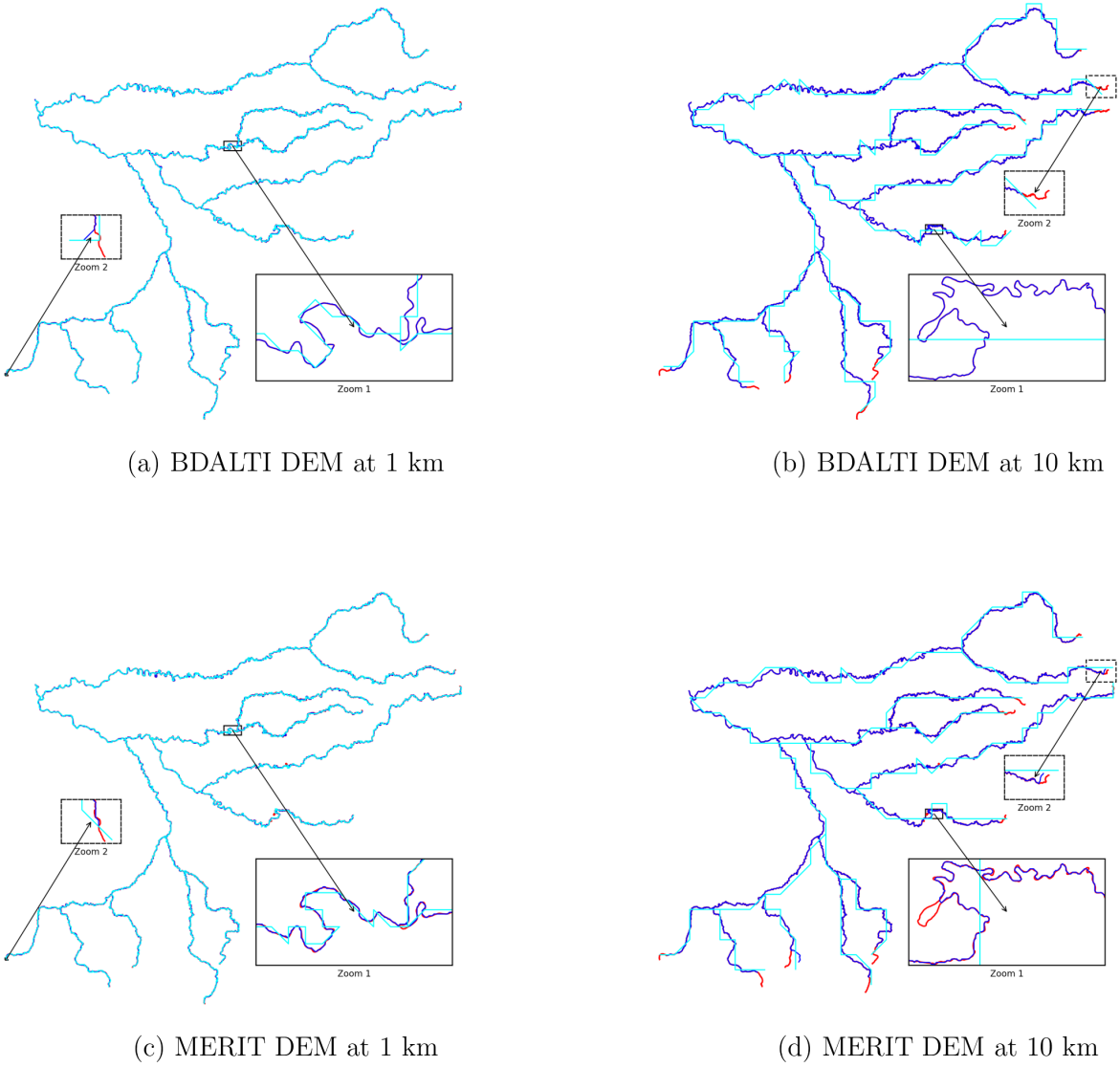

(a) BDALTI DEM at 1 km

(b) BDALTI DEM at 10 km

(c) MERIT DEM at 1 km

(d) MERIT DEM at 10 km

Figure 5. Geometric analysis of preprocessing: Visual comparison of coarse-resolution networks (in cyan), sub-grid networks (in blue) and reference network (in red) for BDALTI and MERIT DEMs at 1 km and 10 km resolutions: (a) BDALTI DEM at 1 km; (b) BDALTI DEM at 10 km; (c) MERIT DEM at 1 km; (d) MERIT DEM at 10 km. Zoom 1 (solid black rectangle) in each map shows inset views of interior basin areas, while Zoom 2 (dashed black rectangle) focuses on headwater regions. The scale bar applies to the four overview maps.

https://doi.org/10.5194/egusphere-2026-1557
Preprint. Discussion started: 27 March 2026

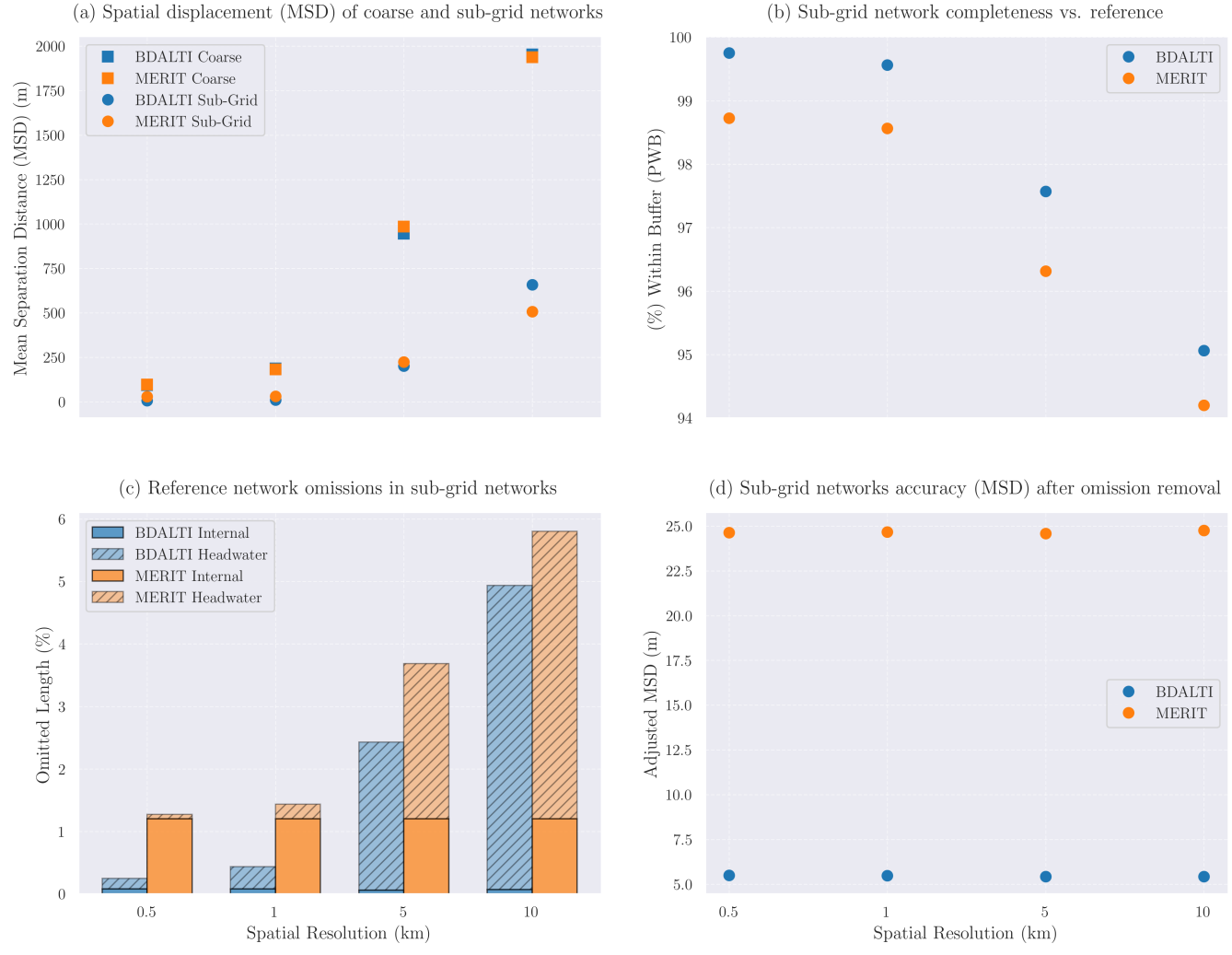

Figure 6. Geometric analysis of preprocessing: Quality assessment of DEM-derived river networks across scales at 100 m burning depth: (a) Mean Separation Distance (MSD) between the reference network and processed networks, for both coarse and sub-grid networks; (b) Percentage Within Buffer indicating the proportion of the reference network captured by the sub-grid network, using a buffer width equal to the native DEM resolution (25 m for BDALTI and 100 m for MERIT); (c) Percentage of omitted reference network length by sub-grid networks (complementary to PWB, i.e., PWB + Omitted Length = 100%); (d) MSD after removing omissions for sub-grid networks.

https://doi.org/10.5194/egusphere-2026-1557
Preprint. Discussion started: 27 March 2026

error interval. Drainage area estimation errors reached up to 219% for the grid-based method, whereas the sub-grid method limits the maximum error to 20%. For the grid-based approach, BDALTI generally yields lower catchment area errors than MERIT, particularly at coarser resolutions (5–10 km), while the sub-grid method produces similar error distributions for both DEMs across scales.

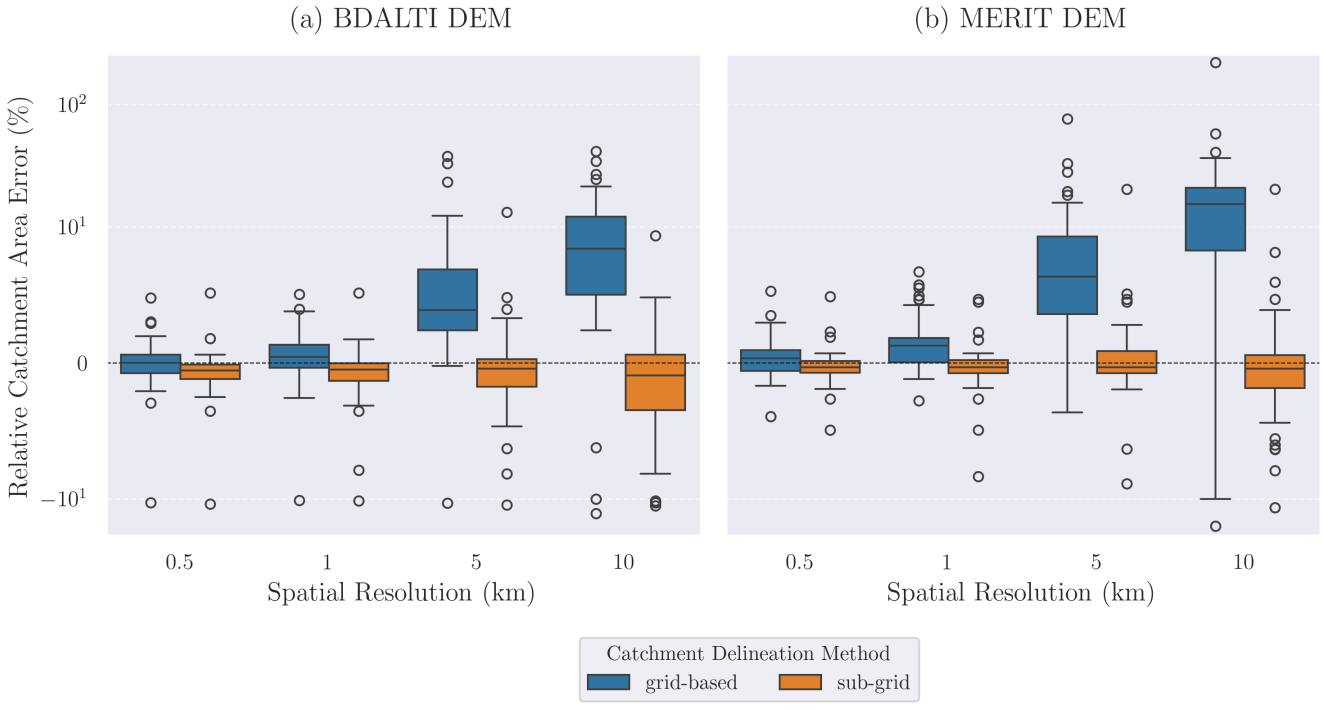

Figure 7. Geometric analysis of preprocessing: Distribution of relative catchment area errors for 44 gauge stations across spatial resolutions, comparing grid-based and sub-grid delineation methods. Errors are computed relative to reference drainage areas at gauging stations: (a) BDALTI DEM; (b) MERIT DEM.

5.3 H&H Model performance across scales

The performance metrics presented in this section are computed from the simulated discharge produced by the complete H&H modeling chain (i.e., $Q(x,t)$) at 18 gauging stations. Figure 8 presents the distribution of KGE′ and its components (Pearson correlation r, variability ratio γ, and bias ratio β) across spatial resolutions and drainage area delineation methods for both DEMs. Performance metrics were computed using the optimal CFL coefficients selected according to the 1% gain threshold described in Section 4.2.2, leading to $\alpha_{\text{CFL}} = 0.9$ for all cases, except for the MERIT 10 km configuration where $\alpha_{\text{CFL}} = 0.7$ is selected for the grid-based method and $\alpha_{\text{CFL}} = 0.2$ for the sub-grid method. Median performance metrics are reported in Table 1, while optimal CFL values, simulation times, and mass balance statistics are summarized in Table 2. For both DEMs, KGE′ distributions remain globally stable across spatial resolutions and drainage area delineation methods (Fig. 8a) with

https://doi.org/10.5194/egusphere-2026-1557
Preprint. Discussion started: 27 March 2026

median values ranging between 0.56 and 0.61 for all configurations (Table 1). The analysis of KGE′ components shows that the Pearson correlation r remains consistently high across all configurations (Fig. 8b,f), with median values between 0.86 and 0.90 (Table 1). Similarly, the variability ratio γ shows limited sensitivity across spatial resolutions and drainage area delineation methods for both DEMs (Fig. 8c,g), with median values ranging between 1.29 and 1.39 (Table 1). In contrast, the bias ratio β displays distinct patterns between the two methods. The grid-based method produces median bias values closer to the ideal value of 1 (ranging from 0.78 to 0.91), while the sub-grid method yields lower bias values (0.71 to 0.80). However, the grid-based method displays a scale-dependent pattern with systematic increase in both median bias and dispersion as spatial resolution coarsens, while the sub-grid method maintains more stable and bounded bias distributions across scales (Fig. 8d,h). Figure 9 illustrates simulated discharge at three representative stations (locations shown in Figures D2) for BDALTI DEM, showing that the model captures the main hydrological patterns across spatial resolutions and drainage area methods. Similar hydrograph patterns for MERIT DEM are shown in Figure D4 (Appendix D). Mass balance conservation between the hydrological domain Ω_{rr} and the hydraulic river network domain Ω_{hy} is consistently ensured across all simulations, with median mass balance errors E_t in the order of 10^{-10} to 10^{-9}, and maximum values do not exceed 10^{-6} for all configurations (Table 2). Computational efficiency improves substantially as spatial resolution coarsens, with simulation times dropping from approximately 4 minutes at 1 km resolution to a few seconds at 5 km and 10 km resolutions (Table 2).

Table 1. Median KGE′ and its components computed from simulated discharge over 18 gauged stations at optimal α_{CFL} values ($\alpha_{\text{CFL}} = 0.9$ for all configurations except MERIT 10 km grid ($\alpha = 0.7$) and sub-grid ($\alpha = 0.2$)).

DEM	Scale	KGE′		r (Correlation)		γ (Variability)		β (Bias)	
		Grid	Sub-grid	Grid	Sub-grid	Grid	Sub-grid	Grid	Sub-grid
BDALTI	1 km	0.61	0.61	0.90	0.90	1.31	1.30	0.78	0.77
	5 km	0.59	0.60	0.89	0.90	1.35	1.31	0.84	0.74
	10 km	0.61	0.59	0.89	0.90	1.32	1.29	0.84	0.71
MERIT	1 km	0.60	0.60	0.90	0.90	1.31	1.31	0.83	0.80
	5 km	0.58	0.58	0.89	0.90	1.34	1.32	0.89	0.80
	10 km	0.56	0.58	0.86	0.89	1.39	1.33	0.91	0.73

6 Discussion

6.1 Coarse vs. sub-grid networks spatial accuracy across scales

The geometric quality assessment of derived networks for both DEMs across scales, performed through both qualitative visual inspection and quantitative metrics (Figure 5 and Figure 6a), confirms the strong resolution dependency of coarse DEM-derived networks, with spatial misalignment increasing as the grid is coarsened, as widely documented in previous studies (e.g., McMaster, 2002; Davies and Bell, 2009; Sousa and Paz, 2017). Achieving better spatial alignment therefore requires

https://doi.org/10.5194/egusphere-2026-1557
Preprint. Discussion started: 27 March 2026

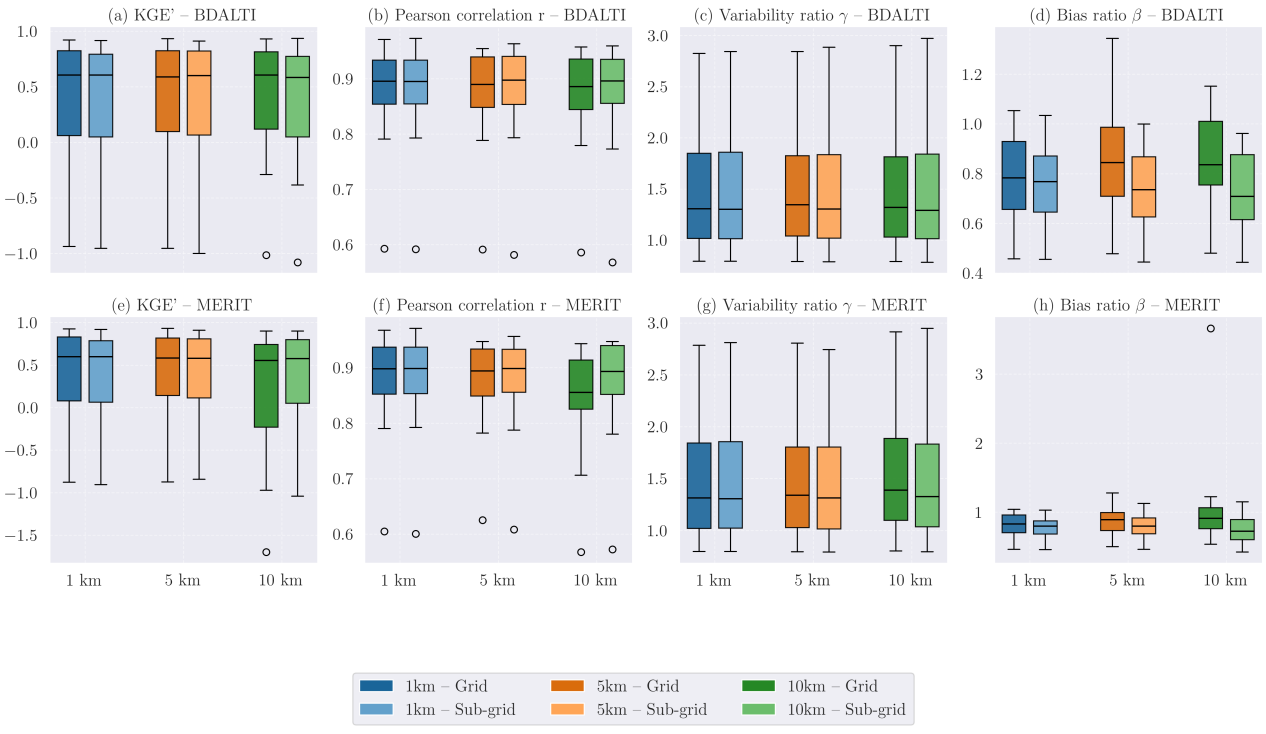

Figure 8. H&H model assessment: Distribution of performance scores for KGE′, Pearson correlation r, variability ratio γ, and bias ratio β computed from simulated discharge at 18 gauging stations for BDALTI and MERIT DEMs across spatial resolutions, using the optimal α_{CFL} value for each simulation configuration ($\alpha_{\text{CFL}} = 0.9$ for all cases, except for the MERIT 10 km configuration where $\alpha_{\text{CFL}} = 0.7$ for the grid-based method and $\alpha_{\text{CFL}} = 0.2$ for the sub-grid method).

Table 2. Optimal CFL coefficients, simulation times, and mass balance statistics for each simulation configuration.

DEM	Scale	α_{CFL}		Sim. Time (s)		E_t (median)		E_t (max)	
		Grid	Sub-grid	Grid	Sub-grid	Grid	Sub-grid	Grid	Sub-grid
BDALTI	1 km	0.9	0.9	226.0	224.9	-2.0e-09	-1.5e-09	4.0e-06	4.3e-06
	5 km	0.9	0.9	12.7	12.3	-3.9e-10	-2.0e-10	1.4e-06	1.6e-06
	10 km	0.9	0.9	1.9	1.9	-5.6e-10	-5.7e-11	9.6e-07	8.8e-07
MERIT	1 km	0.9	0.9	252.8	254.7	-2.7e-09	-2.6e-09	3.7e-06	4.5e-06
	5 km	0.9	0.9	6.3	6.1	0.0e+00	5.9e-10	1.4e-06	1.7e-06
	10 km	0.7	0.2	1.7	2.7	-8.9e-10	-3.6e-11	8.0e-07	1.1e-06

https://doi.org/10.5194/egusphere-2026-1557
Preprint. Discussion started: 27 March 2026

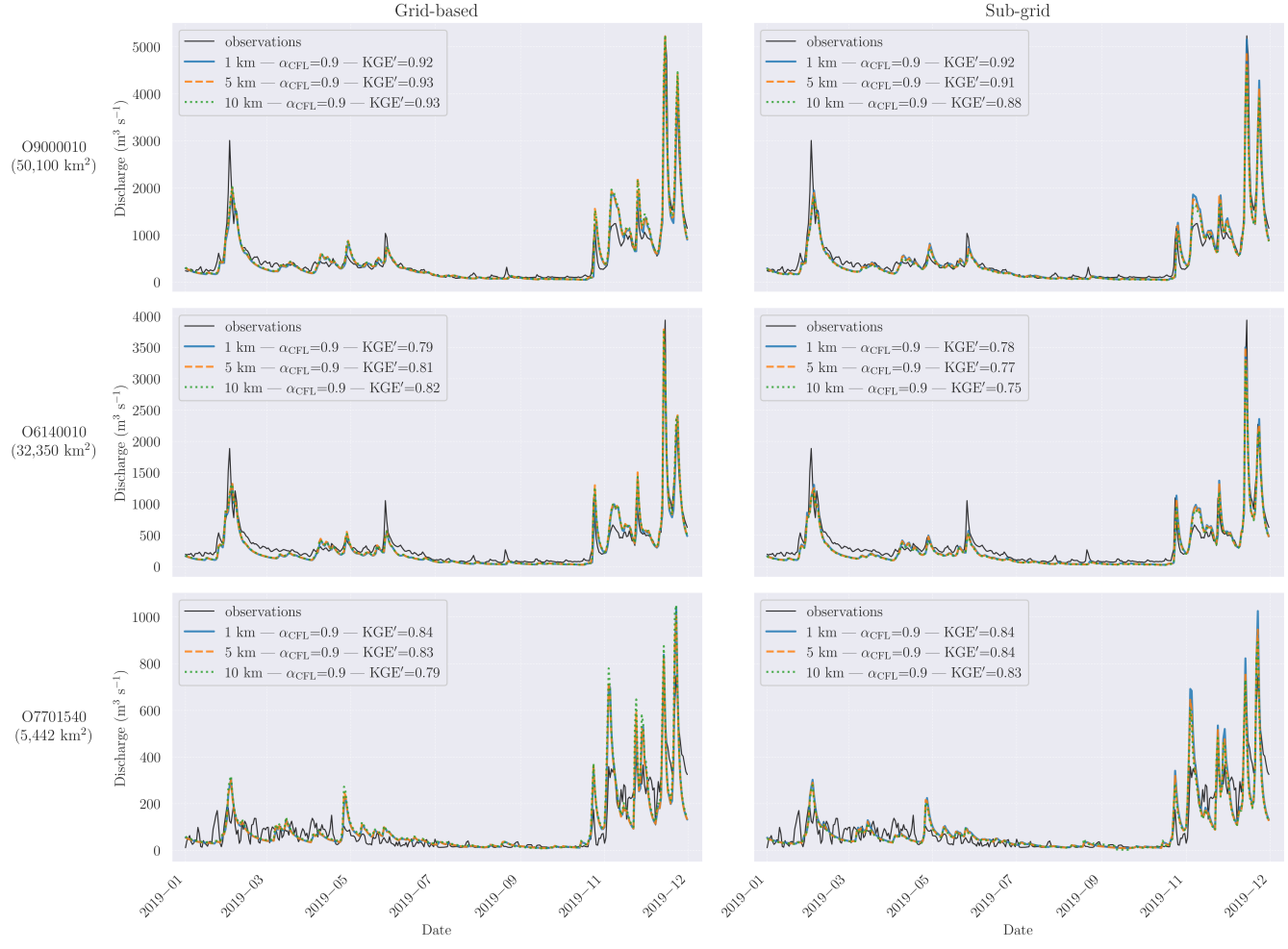

Figure 9. Simulated discharge hydrographs for BDALTI DEM at three selected stations (O9000010, O6140010, O7701540) across spatial resolutions (1 km, 5 km, 10 km) and drainage area delineation methods (grid-based and sub-grid). Rows represent individual stations, columns correspond to area delineation methods (left: grid-based, right: sub-grid). Legend labels indicate spatial resolution, α_{CFL} coefficient and KGE′ performance metric. Station locations are indicated in Figure D2.

https://doi.org/10.5194/egusphere-2026-1557
Preprint. Discussion started: 27 March 2026

finer grid resolution, but this comes at the expense of higher computational costs for modeling. In contrast, sub-grid networks, derived at the native DEM resolutions (25 m for BDALTI and 100 m for resampled MERIT), maintain much higher spatial accuracy across scales. The accuracy decline observed at coarser scales (5–10 km) is directly linked to the decrease in the PWB metric (Figure 6b), indicating that greater parts of the reference network are not captured. The spatial distribution of reference network omissions in Figure 6c reveals two distinct mechanisms. Internal omissions ($\sim$1% for MERIT) result from the DEM's native resolution failing to capture sharp meanders of the reference network, as illustrated in Zoom 1 of Figure 5d. In contrast, headwater omissions (up to $\sim$5% at 10 km for both DEMs) are inherent to the sub-grid delineation approach, which connects outlet pixels of coarse river cells along the fine-resolution flow direction map (see Figure 2), thereby missing headwater segments extending upstream of the outlet pixel of the headwater coarse cell (visible in Zoom 2 of Figure 5). The stabilization of MSD at very low values when omissions are excluded (Figure 6d) confirms that the sub-grid approach maintains consistent spatial accuracy where the network is captured. Overall, this analysis demonstrates that sub-grid representation effectively decouples river network quality from grid resolution, maintaining high spatial accuracy while omitting only a small fraction of the mapped network ($<$6%). This should enable significant computational efficiency gains for large-scale hydrological modeling, as spatial accuracy primarily depends on the native DEM resolution rather than the computational grid resolution.

6.2 Mitigating catchment size errors

The results demonstrate that incorporating fine-resolution drainage boundaries into the hydrological mesh via the sub-grid method substantially improves catchment area estimation accuracy, compared to the conventional grid-based approach, where discrepancies between real drainage boundaries and regular square cell delineation increase as resolution is coarsened. It should be noted that the accuracy of the sub-grid method remains sensitive to the station allocation strategy. Stations are assigned to outlet pixels of coarse river grid cells, and the distance between a gauging station and its associated outlet pixel increases as grid resolution is coarsened, which tends to increase the difference between sub-grid and reference catchment areas. Nevertheless, this approach yields excellent accuracy and represents a practical trade-off between accuracy and algorithmic complexity, compared to a fully vector-based allocation method that would assign stations to the best-fitting pixel on the sub-grid river network, effectively resolving cases where stations are located at multiple confluences within a single grid cell (Godet et al., 2024). The raster-based method is sensitive to DEM native resolution, showing higher errors at coarser scales for MERIT than BDALTI and highlighting the need for high spatial resolution topography for accurate grid-based catchment delineation. In contrast, the sub-grid method provides consistent accuracy across scales for both DEMs, enabling computational efficiency in mesh processing. By explicitly propagating sub-grid drainage areas into the hydrological model (through the computation of lateral inflows Q_{lat}, see Section 2.3.2), we substantially reduce catchment area errors associated with the well-documented "catchment size problem" at coarse resolutions, a major source of bias in multi-scale streamflow modeling and water budget calculations (Yamazaki et al., 2009; Shrestha et al., 2025).

https://doi.org/10.5194/egusphere-2026-1557
Preprint. Discussion started: 27 March 2026

6.3 Understanding multi-scale performance patterns

The KGE′ analysis of simulated discharge shown in Figure 8 reveals that performance differences between area delineation methods across resolutions for both DEMs are primarily driven by the bias ratio β rather than by correlation r or variability γ. The limited sensitivity of correlation r across scales (median values 0.86–0.90), with more than 94% of stations exceeding the 0.6 threshold indicative of good model-observation agreement (Towner et al., 2019), confirms that the routing scheme preserves flow timing independently of drainage area representation. This is consistent since both area delineation methods employ the same sub-grid network across scales with uniform Manning coefficients ($n = 0.05$) and geomorphological channel parametrization (widths, depths, bathymetry). This result therefore further supports the efficiency of the sub-grid network delineation demonstrated in the preprocessing geometric analysis (Figures 5 and 6). The variability ratio γ also shows limited sensitivity across spatial resolutions and between drainage area delineation methods. Notably, by decoupling bias from variability through the use of γ instead of the standard deviation ratio α, KGE′ limits counterbalancing errors inherent to the original KGE where variability and bias are cross-correlated (Cinkus et al., 2023), thereby isolating the bias ratio β as the primary driver of performance differences across spatial resolutions and between area delineation methods. Indeed, the observed sensitivity of the bias component β for the grid-based delineation method reflects the impact of drainage area misrepresentation at coarse resolutions, as demonstrated in Figure 7, which propagates as precipitation volume biases into runoff production. While the grid-based method tends to produce bias values closer to the ideal value of 1, this apparent advantage reflects compensation effects where drainage area overestimation inflates precipitation volumes, partially offsetting the underestimation of streamflow resulting from the combined effects of precipitation aggregation and hydrological parameter smoothing during spatial upscaling. By preserving realistic drainage boundaries, the sub-grid delineation method constrains these volume biases, leading to more stable model performance across spatial resolutions. As illustrated by the hydrographs for BDALTI (Figure 9) and MERIT (Appendix D, Figure D4) at three representative stations, simulated discharges reproduce observed patterns across spatial resolutions for all configurations at their respective optimal α_{CFL}. Additional performance analyses are provided in Appendix D with distributions of the original KGE and its components (r, α, β) (Figure D1) showing correlated bias and variability sensitivities with increased instability across scales for the grid-based delineation method. It is important to note that model performance at the 1 km baseline includes stations with poor performance (negative KGE′ values), primarily due to spatial mismatch between sub-basins used for uniform hydrological parameterization and the 18 evaluation stations considered in this study (only 5 stations coincide with calibration sub-basins). As no recalibration was performed when coarsening the spatial resolution, these poorly performing stations persist or deteriorate when coarsening, as illustrated in the cartographic analysis presented in Appendix D (Figure D2 and D3), which shows the spatial distribution of station performance across scales for both DEMs and highlights the parameterization-evaluation mismatch. Notably, the sensitivity of model performance to the CFL coefficient α_{CFL} increases at coarse resolution, as illustrated by the MERIT 10 km configuration, which requires lower α_{CFL} values (0.7 for the grid-based method and 0.2 for the sub-grid method) to achieve optimal performance, compared to $\alpha_{\text{CFL}} = 0.9$ for all other cases. This increased sensitivity is directly related to the sparser hydraulic discretization at 10 km resolution (Table C1, Appendix C), where larger distances between cross-sections result in larger hydraulic time steps (Equa-

https://doi.org/10.5194/egusphere-2026-1557
Preprint. Discussion started: 27 March 2026

tion A6). Lower α_{CFL} values compensate for this by enforcing smaller hydraulic time steps, thereby improving the accuracy of hydrodynamic calculations. Future developments will therefore focus on optimizing the trade-off between spatial representation, hydrodynamic precision, and computational efficiency by introducing intermediate cross-sections to achieve more uniform spacing along the river network. Furthermore, the excellent mass balance conservation reflects the effectiveness of the direct hydrological–hydraulic coupling, relying on explicit cell-to-cell index matching between raster and vector domains. Despite the aforementioned limitations and although no recalibration was performed at coarser resolutions, these results highlight the strong potential of the proposed H&H modeling framework for large-scale applications.

7 Conclusions

This study presented a raster-vector hydrological-hydraulic (H&H) modeling framework that couples coarse-resolution hydrological grids with fine-scale vector-based river hydrodynamics through a sub-grid representation of both river networks and drainage areas. The framework covers the complete chain from DEM preprocessing to coupled H&H simulations within a unified modeling environment (`smash`). A case application on the Garonne river basin demonstrated through geometric preprocessing analysis that leveraging sub-grid topographic information maintains consistent spatial representation of DEM-derived river networks across scales (0.5 km, 1 km, 5 km, and 10 km) while preserving realistic drainage areas, in contrast to the grid-based discretization that introduces scale-dependent spatial distortions. A simplified H&H modeling experiment was conducted at 1 km, 5 km, and 10 km resolutions without recalibration at coarser scales, maintaining identical hydrological parameterization (through simple parameter upscaling) and uniform hydraulic parameters across all configurations. The H&H simulations confirmed the hydrological relevance of the geometric consistency by preserving flow timing across spatial scales and maintaining more stable hydrological response when using sub-grid drainage areas compared to grid-based areas that exhibited scale-dependent volume biases. The framework's unified architecture, internally coupling hydrological and hydraulic models, enables integrated optimization strategies that account for synergies between hydrological and hydraulic parameters, allowing coupled inference of H&H parameters through hydraulic information feedback to the hydrological model. This is particularly relevant for leveraging emerging water surface observations, such as the SWOT River Database (SWORD) providing a vector-based global river network with high-resolution water surface elevation (WSE) data. The demonstrated spatial consistency between DEM-derived sub-grid networks and reference hydrography facilitates the incorporation of SWOT-derived WSE by seamlessly mapping SWORD nodes to the sub-grid network's computational cross-sections, paving the way for more physically coherent inference of H&H model parameters. Future work will also focus on improving hydraulic parameterization by incorporating channel widths derived from remote sensing products such as Sentinel-1 imagery or LiDAR data to refine river geometry representation at the network scale. The modular structure of the framework within the `smash` environment offers opportunities to evolve toward complete two-directional coupling where hydrodynamic processes dynamically influence hydrological processes, with perspectives to integrate more physically based hydrological models and full Saint-Venant routing schemes.

https://doi.org/10.5194/egusphere-2026-1557
Preprint. Discussion started: 27 March 2026

Code and data availability. The version of `smash` used in this study, implementing the raster–vector hydrological–hydraulic modeling framework, together with the input datasets and analysis scripts required to reproduce the results presented in this paper, is available as a frozen archive on Zenodo at https://doi.org/10.5281/zenodo.18924808 (Berkaoui et al., 2026) (last access: 19 March 2026). The `smash` source code is also available on GitHub at https://github.com/DassHydro/smash/tree/raster-vector-hh-framework (last access: 19 March 2026). `smash` is released under the GPL-3.0 license and is developed openly at https://github.com/DassHydro/smash (last access: 19 March 2026), and the documentation is accessible at https://smash.recover.inrae.fr. As the ANTILOPE J+1 precipitation product by Météo-France (Champeaux et al., 2009) is a commercial dataset with restricted access, we provide in the Zenodo archive (Berkaoui et al., 2026) for reproducibility the open-access COMEPHORE precipitation dataset, available at https://www.data.gouv.fr/datasets/reanalyses-comephore/.

https://doi.org/10.5194/egusphere-2026-1557
Preprint. Discussion started: 27 March 2026

Appendix A: Numerical scheme of the 1D hydrodynamic model

The zero-convective inertia approximation of Saint-Venant equations is solved using an explicit finite-difference scheme on a staggered grid where discharge fluxes are computed at interfaces (index $i+1/2$) between cross-sections while water depths are computed at cross-sections centers (index i)). The time step is denoted by Δt.

Momentum equation discretization

Discretizing and rearranging the momentum equation at interface $i+1/2$ gives the explicit discharge update:

$$Q_{i+1/2}^{t+\Delta t} = \frac{Q_{i+1/2}^{t} - g\Delta t A_{i+1/2}^{t} S_{i+1/2}^{t}}{1 + g\Delta t \frac{n^2 \left|Q_{i+1/2}^{t}\right|}{A_{i+1/2}^{t} (R_{i+1/2}^{t})^{4/3}}} \tag{A1}$$

where $S_{i+1/2}^{t}$ is the water surface slope between cross-section i and downstream cross-section $i+1$:

$$S_{i+1/2}^{t} = \frac{(h_i^t + b_i) - (h_{i+1}^t + b_{i+1})}{\Delta x_{i,i+1}} \tag{A2}$$

Following Neal et al. (2012), the flow depth $h_{i+1/2}^{t}$ and width $w_{i+1/2}^{t}$ at the interface are calculated as:

$$h_{i+1/2}^{t} = \max\left(h_i^t + b_i, h_{i+1}^t + b_{i+1}\right) - \max(b_i, b_{i+1}) \tag{A3}$$

$$w_{i+1/2}^{t} = \min(w_i^t, w_{i+1}^t) \tag{A4}$$

And assuming rectangular cross-sections, the flow area and hydraulic radius at the interface are:

$$A_{i+1/2}^{t} = w_{i+1/2}^{t} h_{i+1/2}^{t}, \quad R_{i+1/2}^{t} = \frac{A_{i+1/2}^{t}}{w_{i+1/2}^{t} + 2h_{i+1/2}^{t}} \tag{A5}$$

To ensure numerical stability, a local time step is computed at each hydrological time step following the CFL stability condition (Yamazaki et al., 2013):

$$\Delta t = \min_{i=1..N} \left(\alpha \frac{\Delta x_{i,i+1}}{\sqrt{g h_i}} \right) \tag{A6}$$

where the minimum is taken over all N cross-sections, α is a stability coefficient ranging between 0.2 and 0.9, $\Delta x_{i,i+1}$ is the flow distance and h_i is the flow depth at cross-section i.

Continuity equation discretization

Mass conservation at each cross-section i is ensured by updating the water volume V_i using the discharge fluxes from the momentum equation and lateral hydrological inflows provided by the hydrological model as:

$$V_i^{t+\Delta t} = V_i^t + \Delta t \left(Q_{i-1/2}^{t+\Delta t} - Q_{i+1/2}^{t+\Delta t} + Q_{lat,i}^{t} \right) \tag{A7}$$

https://doi.org/10.5194/egusphere-2026-1557
Preprint. Discussion started: 27 March 2026

where $Q_{i-1/2}^{t+\Delta t}$ is the upstream inflow (either from hydrological boundary conditions or upstream cross-sections), $Q_{i+1/2}^{t+\Delta t}$ is the downstream outflow computed from the momentum equation, and $Q_{lat,i}^{t}$ represents lateral hydrological inflows from routed hillslope runoff and local runoff generated over river cells. The updated water depth is then computed assuming rectangular channel geometry:

$$h_i^{t+\Delta t} = \frac{V_i^{t+\Delta t}}{\Delta x_{i,i+1} w_i} \tag{A8}$$

Boundary and initial conditions

At upstream boundary cross-sections, discharge is provided by the hydrological model inflows $Q_{i-1/2}^{t}$ (upstream inflows). At the downstream boundary (basin outlet), a zero depth condition is applied. Initial conditions are set with zero flow depth and discharge across the entire network: $h_i^{t=0} = 0$ and $Q_{i+1/2}^{t=0} = 0$.

https://doi.org/10.5194/egusphere-2026-1557
Preprint. Discussion started: 27 March 2026

Appendix B: Hydrological model parametrization

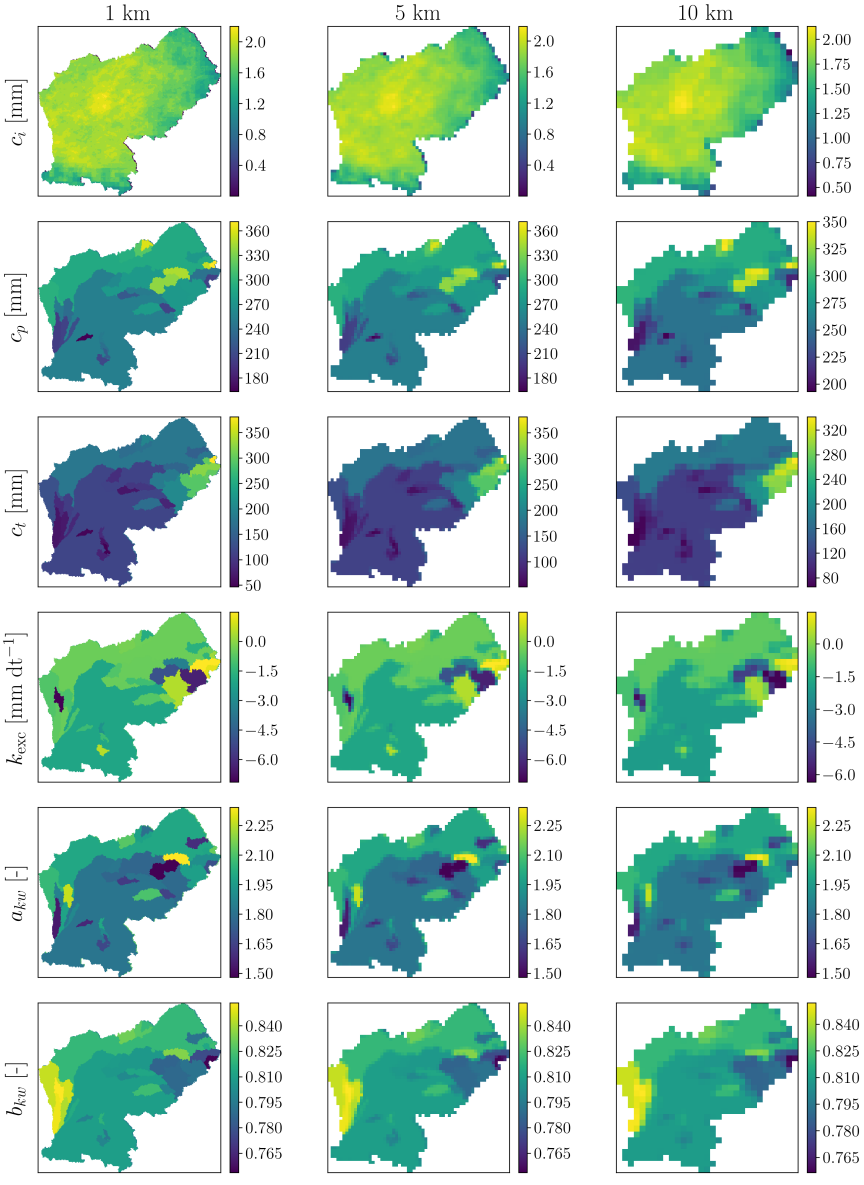

Figure B1. Spatial distribution of hydrological parameters (c_i, c_p, c_t, k_{exc}, a_{kw}, b_{kw}) for BDALTI DEM across resolutions (1 km, 5 km, 10 km). Rows represent parameters and columns represent resolutions. Parameter fields at 5 km and 10 km are obtained by arithmetic mean aggregation of 1 km baseline without recalibration, showing progressive spatial smoothing.

https://doi.org/10.5194/egusphere-2026-1557
Preprint. Discussion started: 27 March 2026

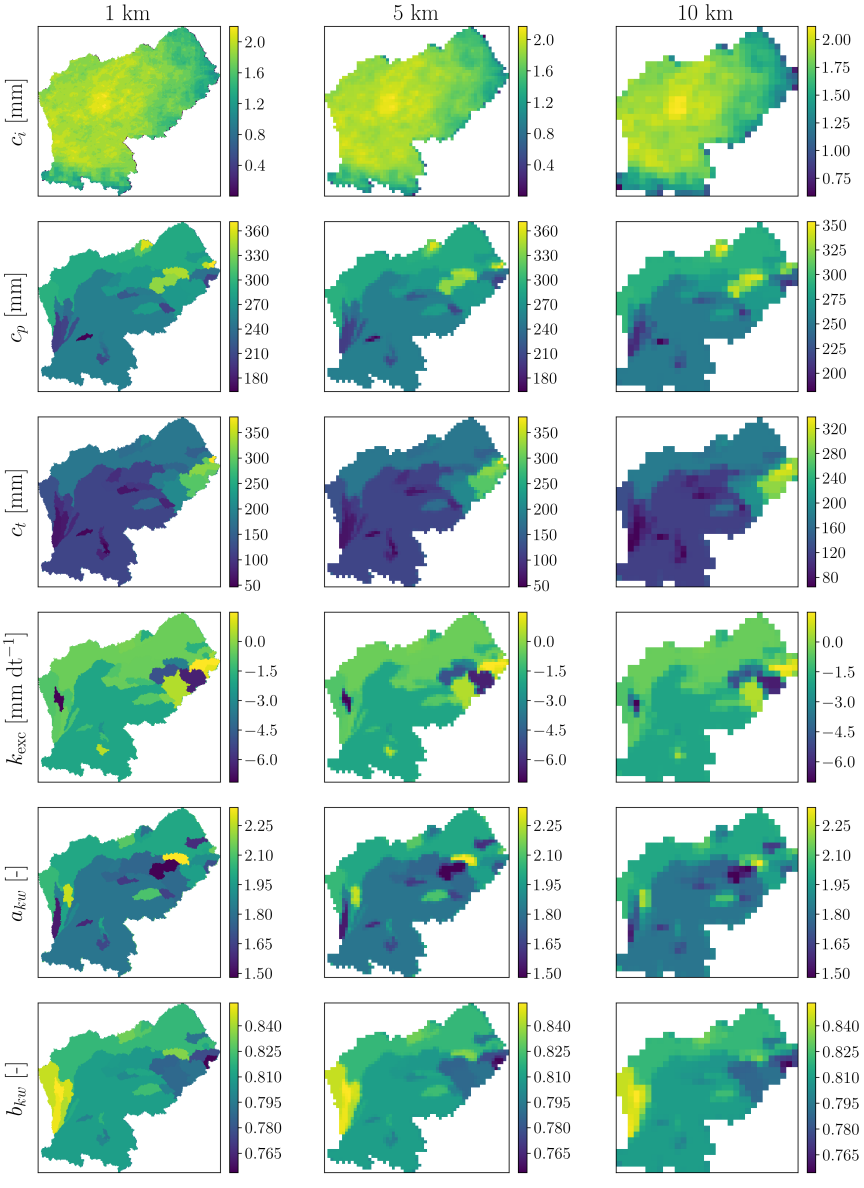

Figure B2. Spatial distribution of hydrological parameters for MERIT DEM across resolutions. Layout and methodology identical to Figure B1.

https://doi.org/10.5194/egusphere-2026-1557
Preprint. Discussion started: 27 March 2026

Appendix C: Hydraulic model parametrization

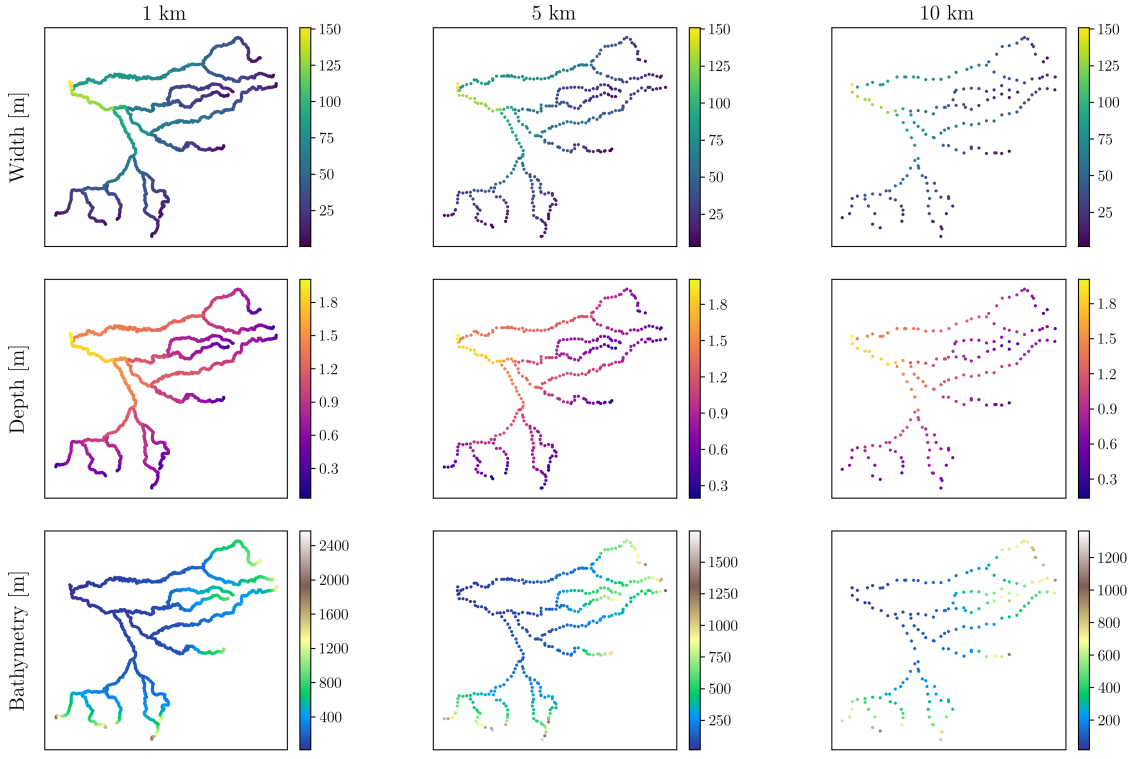

Figure C1. Spatial distribution of hydraulic attributes along the sub-grid network for BDALTI DEM across resolutions (1 km, 5 km, 10 km). Rows represent channel width (w_i), depth (h_i) and bathymetry (b_i) from top to bottom, and columns correspond to spatial resolutions.

Table C1. Summary statistics of flow distances Δx between consecutive hydraulic cross-sections along the sub-grid river network for each DEM and spatial resolution (Q25 stands for the 25th quantile, and Q75 for the 75th quantile).

Configuration	N sections	Min (km)	Q25 (km)	Median (km)	Q75 (km)	Max (km)
BDALTI 1 km	2240	0.03	0.94	1.17	1.41	3.56
BDALTI 5 km	373	0.32	5.54	6.94	8.65	17.47
BDALTI 10 km	173	1.62	12.03	14.71	17.90	31.47
MERIT 1 km	2269	0.10	0.87	1.12	1.33	5.70
MERIT 5 km	375	0.42	5.21	6.52	7.96	17.10
MERIT 10 km	167	2.66	11.97	14.09	17.06	38.14

https://doi.org/10.5194/egusphere-2026-1557
Preprint. Discussion started: 27 March 2026

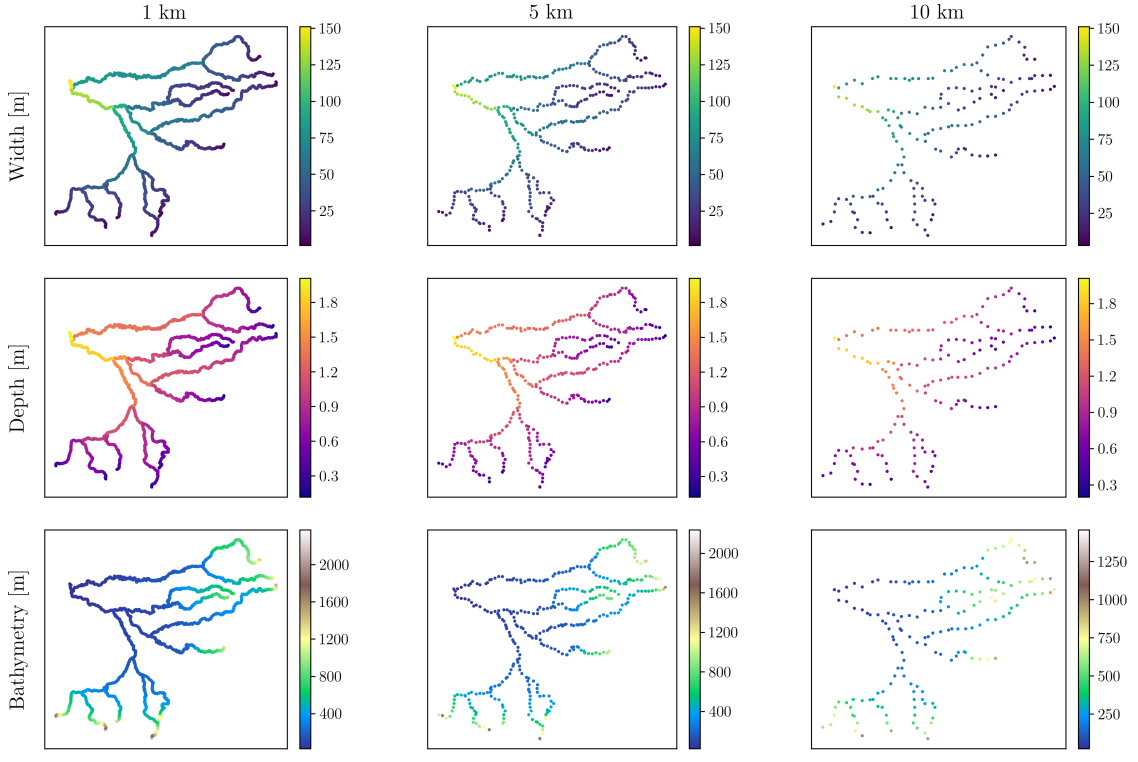

Figure C2. Spatial distribution of hydraulic attributes along the sub-grid network for MERIT DEM across resolutions. Layout and methodology identical to Figure C1.

https://doi.org/10.5194/egusphere-2026-1557
Preprint. Discussion started: 27 March 2026

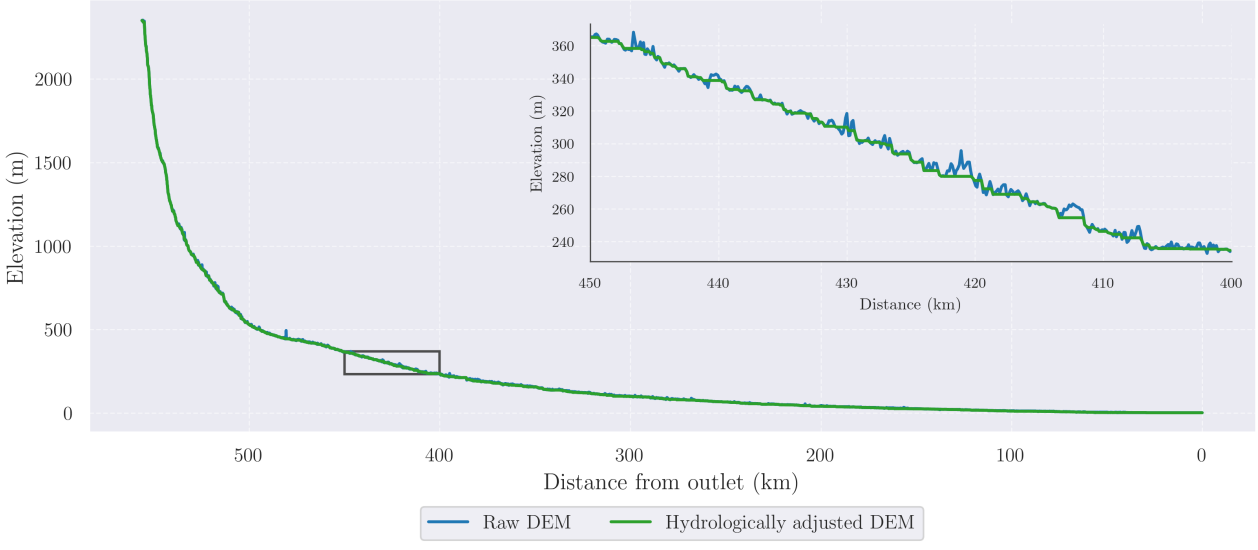

Figure C3. Longitudinal elevation profile of the Garonne river extracted from MERIT DEM before and after hydrological adjustment. Elevations are extracted along the DEM-derived flow path from upstream to downstream. The hydrological adjustment ensures monotonic downstream elevation decrease along the river flow path (in green), eliminating all elevation inversions present in the raw DEM (in blue).

https://doi.org/10.5194/egusphere-2026-1557
Preprint. Discussion started: 27 March 2026

Appendix D: Supplementary performance analysis

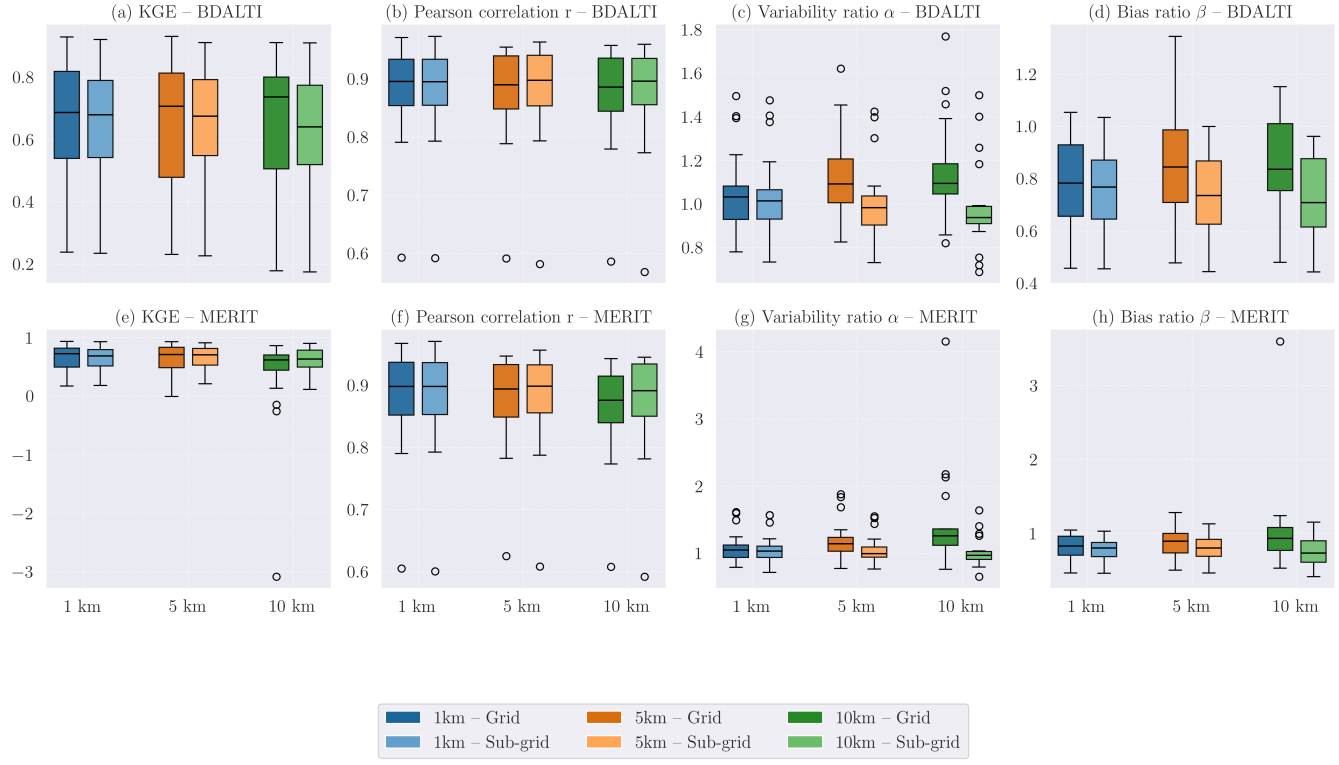

Figure D1. Distribution of original KGE and its components (Pearson correlation r, variability ratio α, bias ratio β) computed from simulated discharge at 18 gauging stations across spatial resolutions and delineation methods. In contrast to KGE′ (see Figure 8) , KGE exhibits correlated responses between variability and bias components, leading to increased dispersion and instability at coarser resolutions, particularly for the grid-based area delineation method. This highlights the advantage of KGE′ in isolating the bias ratio β as the primary driver of performance differences between area delineation methods across scales.

https://doi.org/10.5194/egusphere-2026-1557
Preprint. Discussion started: 27 March 2026

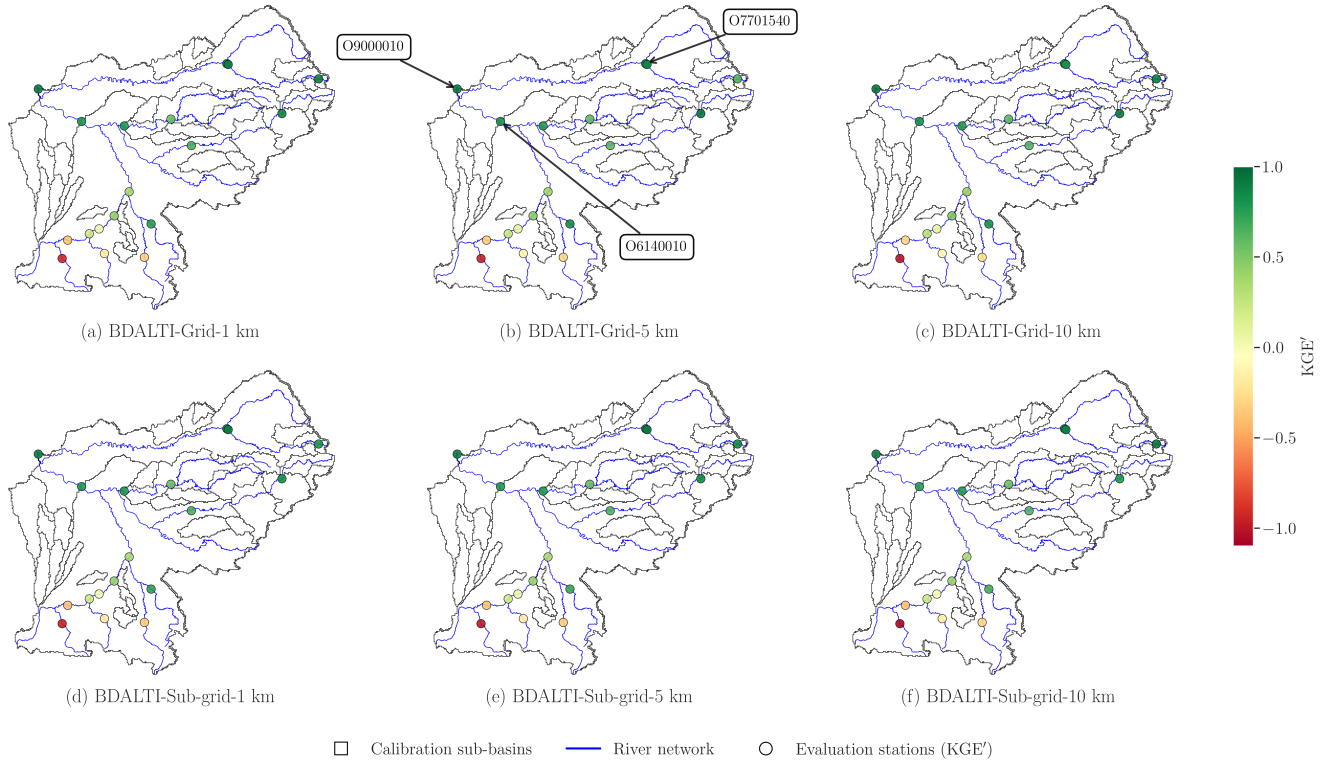

Figure D2. Spatial distribution of KGE′ computed from simulated discharge for BDALTI DEM simulations across spatial resolutions and drainage area delineation methods. Calibration sub-basins used for uniform hydrological parameterization are shown as black polygons, with the reference river network displayed in blue. Station markers are color-coded according to KGE′ values. Hydrographs for three representative stations (O9000010, O6140010, O7701540) annotated on panel (b) are shown in Figures 9.

https://doi.org/10.5194/egusphere-2026-1557
Preprint. Discussion started: 27 March 2026

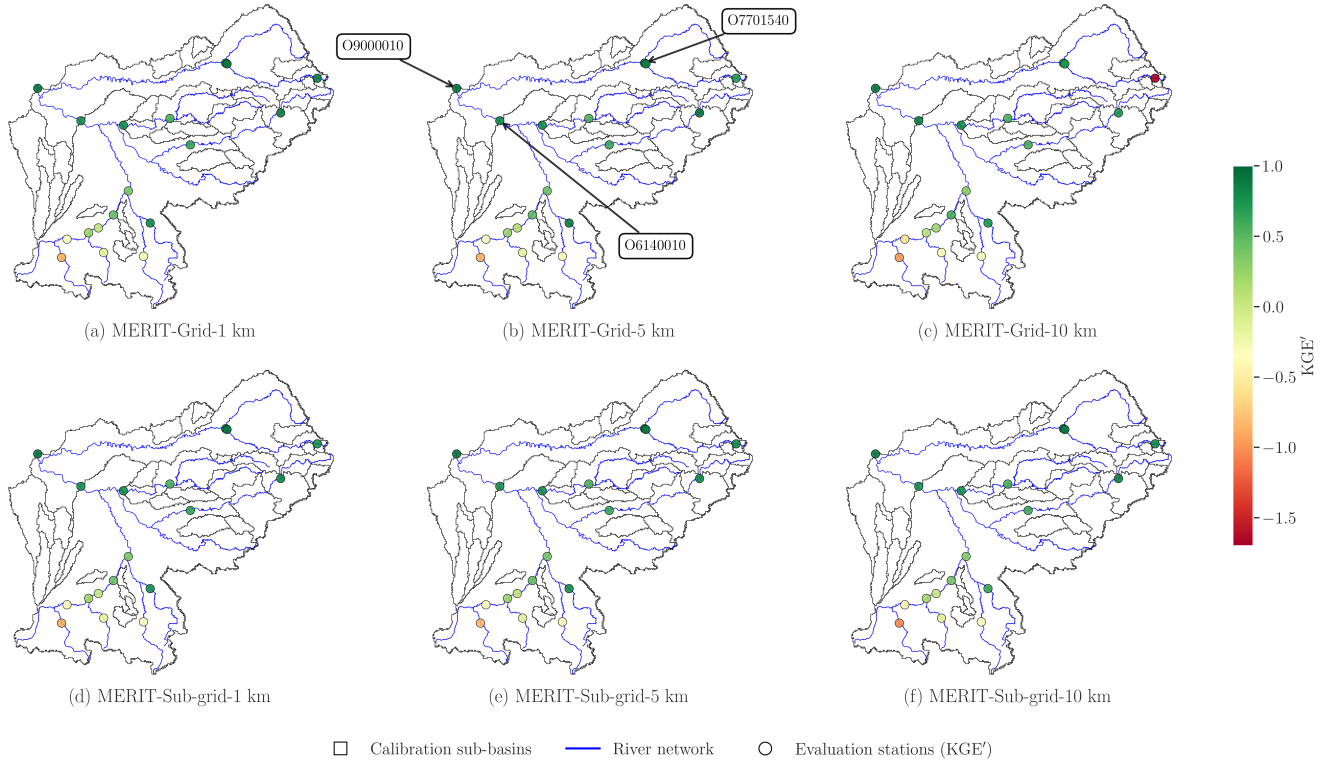

Figure D3. Spatial distribution of KGE′ computed from simulated discharge for MERIT DEM simulations across spatial resolutions and drainage area delineation methods. Layout identical to Figure D2. Hydrographs for three representative stations (O9000010, O6140010, O7701540) annotated on panel (b) are shown in Figures D4.

https://doi.org/10.5194/egusphere-2026-1557
Preprint. Discussion started: 27 March 2026

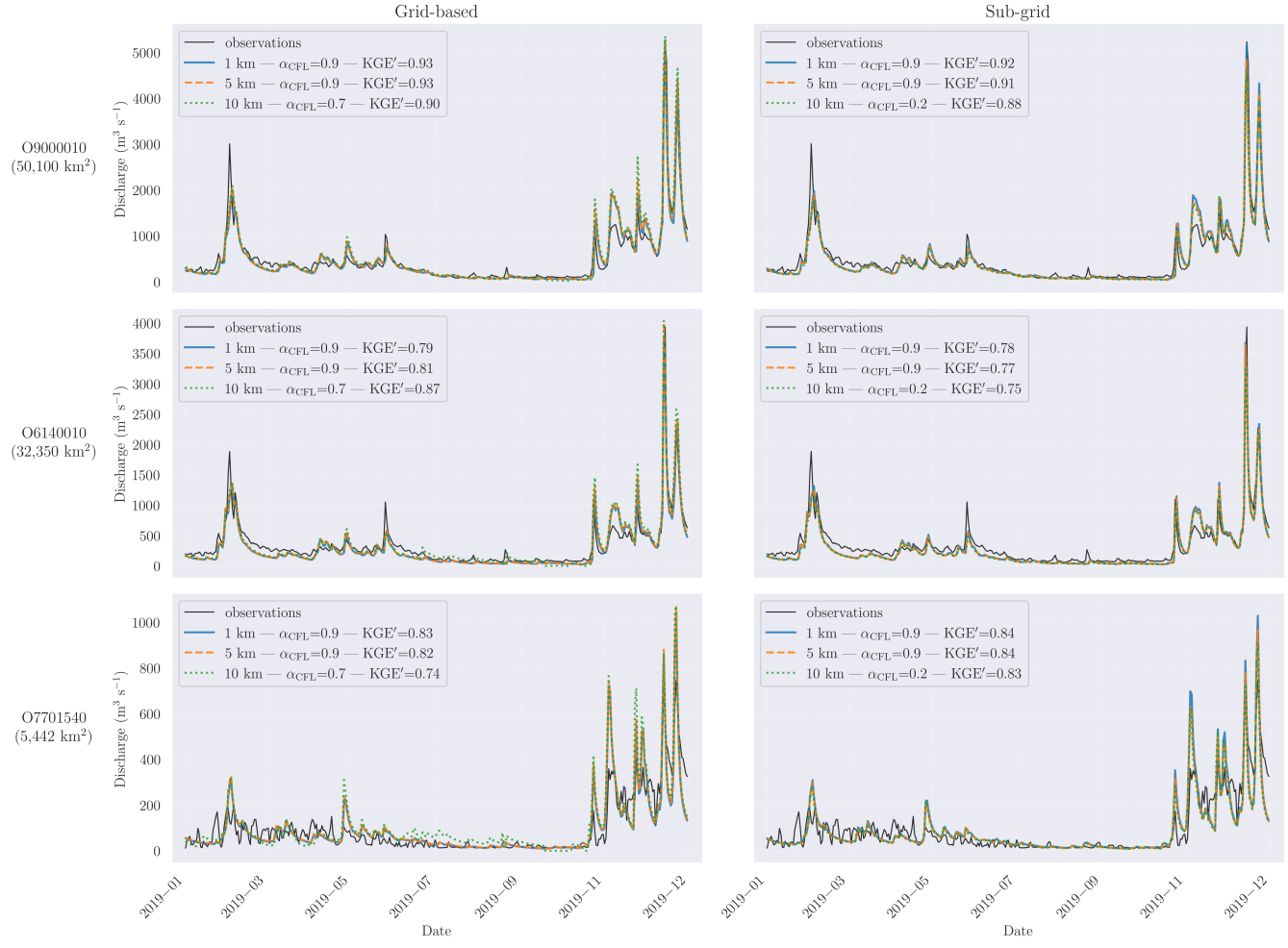

Figure D4. Simulated discharge hydrographs for MERIT DEM at three selected stations (O9000010, O6140010, O7701540) across spatial resolutions (1 km, 5 km, 10 km) and drainage area delineation methods (grid-based and sub-grid). Rows represent individual stations, columns correspond to area delineation methods (left: grid-based, right: sub-grid). Legend labels indicate spatial resolution, α_{CFL} coefficient and KGE′ performance metric. Station locations are indicated in Figure D3.

https://doi.org/10.5194/egusphere-2026-1557
Preprint. Discussion started: 27 March 2026

Author contributions. MAB: conceptualization, methodology, software development, numerical experiments, and writing of the original draft. MS: supervision and manuscript review and editing. FC: software development. NNTH: software development. AA: data provision. KL: conceptualization, methodology, and software development. HR: conceptualization, supervision, funding acquisition, and manuscript review and editing. PAG: conceptualization, methodology, software development, supervision, funding acquisition, and manuscript review and editing.

Competing interests. The authors declare no competing interests

Acknowledgements. This research was supported by the French Office for Biodiversity (OFB - Office Français de la Biodiversité) and by the Agence Nationale de la Recherche MUFFINS project (grant no. ANR-21-CE04-0021-01).

https://doi.org/10.5194/egusphere-2026-1557
Preprint. Discussion started: 27 March 2026

References

Almeida, A. A. R. D., Mendonça, R. L., Silva, N. M. M., and Paz, A. R. d.: Evaluation of LiDAR-derived river networks coarsening with spatial patterns preservation, Computers & Geosciences, 189, 105 639, https://doi.org/10.1016/j.cageo.2024.105639, 2024.

Bates, P. D. and De Roo, A. P. J.: A simple raster-based model for flood inundation simulation, Journal of Hydrology, 236, 54–77, https://doi.org/10.1016/s0022-1694(00)00278-x, 2000.

Bates, P. D., Horritt, M. S., and Fewtrell, T. J.: A simple inertial formulation of the shallow water equations for efficient two-dimensional flood inundation modelling, Journal of Hydrology, 387, 33–45, https://doi.org/10.1016/j.jhydrol.2010.03.027, 2010.

Berkaoui, M. A., Saadi, M., Colleoni, F., Huynh, N. N. T., Akhtari, A., Larnier, K., Roux, H., and Garambois, P.-A.: A Raster–Vector Framework for Multi-Scale Hydrological–Hydraulic Modeling Across Large Domains, Zenodo [code and data], https://doi.org/10.5281/zenodo.18924808, 2026.

Biancamaria, S., Mballo, M., Le Moigne, P., Sánchez Pérez, J. M., Espitalier-Noël, G., Grusson, Y., Cakir, R., Häfliger, V., Barathieu, F., Trasmonte, M., Boone, A., Martin, E., and Sauvage, S.: Total water storage variability from GRACE mission and hydrological models for a 50,000 km2 temperate watershed: the Garonne River basin (France), Journal of Hydrology: Regional Studies, 24, 100 609, https://doi.org/https://doi.org/10.1016/j.ejrh.2019.100609, 2019.

Champeaux, J.-L., Dupuy, P., Laurantin, O., Soulan, I., Tabary, P., and Soubeyroux, J.-M.: Les mesures de précipitations et l'estimation des lames d'eau à Météo-France : état de l'art et perspectives, La Houille Blanche, 95, 28–34, https://doi.org/10.1051/lhb/2009052, 2009.

Chomba, I. C., Banda, K. E., Winsemius, H. C., Chomba, M. J., Mataa, M., Ngwenya, V., Sichingabula, H. M., Nyambe, I. A., and Ellender, B.: A Review of Coupled Hydrologic-Hydraulic Models for Floodplain Assessments in Africa: Opportunities and Challenges for Floodplain Wetland Management, Hydrology, 8, 44, https://doi.org/10.3390/hydrology8010044, 2021.

Chow, V. T., Maidment, D. R., and Mays, L. W.: Applied hydrology, McGraw-Hill series in water resources and environmental engineering, McGraw-Hill, ISBN 978-0-07-010810-3, 1988.

Cinkus, G., Mazzilli, N., Jourde, H., Wunsch, A., Liesch, T., Ravbar, N., Chen, Z., and Goldscheider, N.: When best is the enemy of good – critical evaluation of performance criteria in hydrological models, Hydrology and Earth System Sciences, 27, 2397–2411, https://doi.org/10.5194/hess-27-2397-2023, 2023.

Clark, M. P., Fan, Y., Lawrence, D. M., Adam, J. C., Bolster, D., Gochis, D. J., Hooper, R. P., Kumar, M., Leung, L. R., Mackay, D. S., Maxwell, R. M., Shen, C., Swenson, S. C., and Zeng, X.: Improving the representation of hydrologic processes in Earth System Models, Water Resources Research, 51, 5929–5956, https://doi.org/10.1002/2015wr017096, 2015.

Colleoni, F., Garambois, P.-A., Javelle, P., Jay-Allemand, M., and Arnaud, P.: Adjoint-based spatially distributed calibration of a grid GR-based parsimonious hydrological model over 312 French catchments with SMASH platform, EGUsphere, 2022, 1–37, https://doi.org/10.5194/egusphere-2022-506, 2022.

Colleoni, F., Huynh, N. N. T., Garambois, P.-A., Jay-Allemand, M., Organde, D., Renard, B., De Fournas, T., El Baz, A., Demargne, J., and Javelle, P.: SMASH v1.0: a differentiable and regionalizable high-resolution hydrological modeling and data assimilation framework, Geoscientific Model Development, 18, 7003–7034, https://doi.org/10.5194/gmd-18-7003-2025, 2025.

Coppo Frias, M., Vesterhauge, A. R., Olesen, D. H., Bandini, F., Grosen, H., Nielsen, S. Y., and Bauer-Gottwein, P.: Combining UAS LiDAR, Sonar, and Radar Altimetry for River Hydraulic Characterization, Drones, 9, 31, https://doi.org/10.3390/drones9010031, 2025.

Davies, H. N. and Bell, V. A.: Assessment of methods for extracting low-resolution river networks from high-resolution digital data, Hydrological Sciences Journal, 54, 17–28, https://doi.org/10.1623/hysj.54.1.17, 2009.

https://doi.org/10.5194/egusphere-2026-1557
Preprint. Discussion started: 27 March 2026

Dey, S., Saksena, S., and Merwade, V.: Assessing the effect of different bathymetric models on hydraulic simulation of rivers in data sparse regions, Journal of Hydrology, 575, 838–851, https://doi.org/10.1016/j.jhydrol.2019.05.085, 2019.

Dey, S., Saksena, S., Winter, D., Merwade, V., and McMillan, S.: Incorporating Network Scale River Bathymetry to Improve Characterization of Fluvial Processes in Flood Modeling, Water Resources Research, 58, e2020WR029 521, https://doi.org/10.1029/2020wr029521, 2022.

Eilander, D.: pyFlwDir, https://doi.org/10.5281/zenodo.6108034, 2022.

Eilander, D., van Verseveld, W., Yamazaki, D., Weerts, A., Winsemius, H. C., and Ward, P. J.: A hydrography upscaling method for scale-invariant parametrization of distributed hydrological models, Hydrology and Earth System Sciences, 25, 5287–5313, https://doi.org/10.5194/hess-25-5287-2021, 2021.

Fleischmann, A., Siqueira, V., Paris, A., Collischonn, W., Paiva, R., Pontes, P., Crétaux, J.-F., Bergé-Nguyen, M., Biancamaria, S., Gosset, M., Calmant, S., and Tanimoun, B.: Modelling hydrologic and hydrodynamic processes in basins with large semi-arid wetlands, Journal of Hydrology, 561, 943–959, https://doi.org/10.1016/j.jhydrol.2018.04.041, 2018.

Garambois, P.-A. and Monnier, J.: Inference of effective river properties from remotely sensed observations of water surface, Advances in Water Resources, 79, 103–120, https://doi.org/https://doi.org/10.1016/j.advwatres.2015.02.007, 2015.

Getirana, A. C. V., Bonnet, M.-P., Rotunno Filho, O. C., and Mansur, W. J.: Improving hydrological information acquisition from DEM processing in floodplains, Hydrological Processes, 23, 502–514, https://doi.org/10.1002/hyp.7167, 2009.

Gharari, S., Clark, M. P., Mizukami, N., Knoben, W. J. M., Wong, J. S., and Pietroniro, A.: Flexible vector-based spatial configurations in land models, Hydrology and Earth System Sciences, 24, 5953–5971, https://doi.org/10.5194/hess-24-5953-2020, 2020.

Godet, J., Gaume, E., Javelle, P., Nicolle, P., and Payrastre, O.: Technical note: Comparing three different methods for allocating river points to coarse-resolution hydrological modelling grid cells, Hydrology and Earth System Sciences, 28, 1403–1413, https://doi.org/10.5194/hess-28-1403-2024, 2024.

Gupta, H. V., Kling, H., Yilmaz, K. K., and Martinez, G. F.: Decomposition of the mean squared error and NSE performance criteria: Implications for improving hydrological modelling, Journal of Hydrology, 377, 80–91, https://doi.org/10.1016/j.jhydrol.2009.08.003, 2009.

Hallouin, T.: hydroeval: an evaluator for streamflow time series in Python (Version 0.1.0). Zenodo, Zenodo, https://doi.org/10.5281/zenodo.4709652, 2021.

Hoch, J. M., Neal, J. C., Baart, F., van Beek, R., Winsemius, H. C., Bates, P. D., and Bierkens, M. F. P.: GLOFRIM v1.0 – A globally applicable computational framework for integrated hydrological–hydrodynamic modelling, Geoscientific Model Development, 10, 3913–3929, https://doi.org/10.5194/gmd-10-3913-2017, 2017.

Hunter, N. M., Bates, P. D., Horritt, M. S., and Wilson, M. D.: Simple spatially-distributed models for predicting flood inundation: A review, Geomorphology, 90, 208–225, https://doi.org/https://doi.org/10.1016/j.geomorph.2006.10.021, 2007.

Huynh, N. N. T., Garambois, P.-A., Colleoni, F., and Javelle, P.: Signatures-and-sensitivity-based multi-criteria variational calibration for distributed hydrological modeling applied to Mediterranean floods, Journal of Hydrology, 625, 129 992, https://doi.org/10.1016/j.jhydrol.2023.129992, 2023.

Huynh, N. N. T., Garambois, P.-A., Colleoni, F., Renard, B., Roux, H., Demargne, J., Jay-Allemand, M., and Javelle, P.: Learning Regionalization Using Accurate Spatial Cost Gradients Within a Differentiable High-Resolution Hydrological Model: Application to the French Mediterranean Region, Water Resources Research, 60, e2024WR037 544, https://doi.org/10.1029/2024WR037544, 2024.

Huynh, N. N. T., Garambois, P.-A., Renard, B., Colleoni, F., Monnier, J., and Roux, H.: A distributed hybrid physics–AI framework for learning corrections of internal hydrological fluxes and enhancing high-resolution regionalized flood modeling, Hydrology and Earth System Sciences, 29, 3589–3613, https://doi.org/10.5194/hess-29-3589-2025, 2025.

https://doi.org/10.5194/egusphere-2026-1557
Preprint. Discussion started: 27 March 2026

Huynh, N. N. T., Garambois, P.-A., Colleoni, F., and Monnier, J.: A hybrid physics–AI approach using universal differential equations with state-dependent neural networks for learnable, regionalizable, spatially distributed hydrological modeling, Geoscientific Model Development, 19, 1055–1074, https://doi.org/10.5194/gmd-19-1055-2026, 2026.

IGN: BD ALTI® Version 2.0 - Descriptif de contenu, Tech. rep., Institut National de l'Information Géographique et Forestière, 2017.

Kling, H., Fuchs, M., and Paulin, M.: Runoff conditions in the upper Danube basin under an ensemble of climate change scenarios, Journal of Hydrology, 424-425, 264–277, https://doi.org/10.1016/j.jhydrol.2012.01.011, 2012.

Kotyra, B. and Chabudziński, L.: Fast parallel algorithms for finding the longest flow paths in flow direction grids, Environmental Modelling & Software, 167, 105 728, https://doi.org/10.1016/j.envsoft.2023.105728, 2023.

Larnier, K., Garambois, P.-A., Emery, C., Pujol, L., Monnier, J., Gal, L., Paris, A., Yesou, H., Ledauphin, T., and Calmant, S.: Estimating Channel Parameters and Discharge at River Network Scale Using Hydrological-Hydraulic Models, SWOT and Multi-Satellite Data, Water Resources Research, 61, e2024WR038 455, https://doi.org/10.1029/2024wr038455, 2025.

Ledauphin, T., Garambois, P.-A., Larnier, K., Azzoni, M., Emery, C., Picot, N., Amzil, S., Fjørtoft, R., Maxant, J., and Yésou, H.: Assessing SWOT's Hydraulic Visibility on the Rhine: Precision Flow Lines and Slope-Based Flood Wave Propagation Signatures, Earth and Space Science, 12, e2025EA004 309, https://doi.org/https://doi.org/10.1029/2025EA004309, 2025.

Lehner, B.: HydroSHEDS Technical Documentation, Tech. rep., World Wildlife Fund US, 2022.

Lehner, B. and Grill, G.: Global river hydrography and network routing: baseline data and new approaches to study the world's large river systems, Hydrological Processes, 27, 2171–2186, https://doi.org/10.1002/hyp.9740, 2013.

Lehner, B., Verdin, K., and Jarvis, A.: New Global Hydrography Derived From Spaceborne Elevation Data, Eos, Transactions American Geophysical Union, 89, 93–94, https://doi.org/10.1029/2008eo100001, 2008.

Li, Z., Chen, M., Gao, S., Luo, X., Gourley, J. J., Kirstetter, P., Yang, T., Kolar, R., McGovern, A., Wen, Y., Rao, B., Yami, T., and Hong, Y.: CREST-iMAP v1.0: A fully coupled hydrologic-hydraulic modeling framework dedicated to flood inundation mapping and prediction, Environmental Modelling & Software, 141, 105 051, https://doi.org/10.1016/j.envsoft.2021.105051, 2021.

Li, Z., Gao, S., Chen, M., Gourley, J., Mizukami, N., and Hong, Y.: CREST-VEC: a framework towards more accurate and realistic flood simulation across scales, Geoscientific Model Development, 15, 6181–6196, https://doi.org/10.5194/gmd-15-6181-2022, 2022.

Lin, P., Pan, M., Wood, E. F., Yamazaki, D., and Allen, G. H.: A new vector-based global river network dataset accounting for variable drainage density, Scientific Data, 8, 28, https://doi.org/10.1038/s41597-021-00819-9, 2021.

Lindsay, J. B.: The practice of DEM stream burning revisited, Earth Surface Processes and Landforms, 41, 658–668, https://doi.org/10.1002/esp.3888, 2016.

Mathevet, T.: Quels modèles pluie-débit globaux au pas de temps horaire ? Développements empiriques et comparaison de modèles sur un large échantillon de bassins versants, phdthesis, ENGREF Paris, https://hal.inrae.fr/tel-02587642, 2005.

McMaster, K. J.: Effects of digital elevation model resolution on derived stream network positions, Water Resources Research, 38, 13–1–13–8, https://doi.org/10.1029/2000wr000150, 2002.

Mizukami, N., Clark, M. P., Sampson, K., Nijssen, B., Mao, Y., McMillan, H., Viger, R. J., Markstrom, S. L., Hay, L. E., Woods, R., Arnold, J. R., and Brekke, L. D.: mizuRoute version 1: a river network routing tool for a continental domain water resources applications, Geoscientific Model Development, 9, 2223–2238, https://doi.org/10.5194/gmd-9-2223-2016, 2016.

Neal, J., Schumann, G., and Bates, P.: A subgrid channel model for simulating river hydraulics and floodplain inundation over large and data sparse areas, Water Resources Research, 48, https://doi.org/10.1029/2012wr012514, 2012.

https://doi.org/10.5194/egusphere-2026-1557
Preprint. Discussion started: 27 March 2026

O'Callaghan, J. F. and Mark, D. M.: The Extraction of Drainage Networks from Digital Elevation Data, Computer Vision, Graphics, and Image Processing, 28, 323–344, https://doi.org/https://doi.org/10.1016/S0734-189X(84)80011-0, 1984.

Oudin, L., Hervieu, F., Michel, C., Perrin, C., Andréassian, V., Anctil, F., and Loumagne, C.: Which potential evapotranspiration input for a lumped rainfall–runoff model?: Part 2—Towards a simple and efficient potential evapotranspiration model for rainfall–runoff modelling, Journal of Hydrology, 303, 290–306, https://doi.org/https://doi.org/10.1016/j.jhydrol.2004.08.026, 2005.

Paiva, R. C. D., Collischonn, W., and Tucci, C. E. M.: Large scale hydrologic and hydrodynamic modeling using limited data and a GIS based approach, Journal of Hydrology, 406, 170–181, https://doi.org/10.1016/j.jhydrol.2011.06.007, 2011.

Pappenberger, F., Beven, K., Horritt, M., and Blazkova, S.: Uncertainty in the calibration of effective roughness parameters in HEC-RAS using inundation and downstream level observations, Journal of Hydrology, 302, 46–69, https://doi.org/https://doi.org/10.1016/j.jhydrol.2004.06.036, 2005.

Pardé, M.: Le Régime de la Garonne, Revue géographique des Pyrénées et du Sud-Ouest. Sud-Ouest Européen, 6, 105–262, https://doi.org/10.3406/rgpso.1935.4186, 1935.

Pella, H., Lejot, J., Lamouroux, N., and Snelder, T.: Le réseau hydrographique théorique (RHT) français et ses attributs environnementaux, Géomorphologie : relief, processus, environnement, 18, 317–336, https://doi.org/10.4000/geomorphologie.9933, 2012.

Perrin, C., Michel, C., and Andréassian, V.: Improvement of a parsimonious model for streamflow simulation, Journal of Hydrology, 279, 275–289, https://doi.org/10.1016/s0022-1694(03)00225-7, 2003.

Piotte, O., Montmerle, T., Fouchier, C., Belleudy, A., Garandeau, L., Janet, B., Jauffret, C., Demargne, J., and Organde, D.: Les évolutions du service d'avertissement sur les pluies intenses et les crues soudaines en France☆, La Houille Blanche, 106, 75–84, https://doi.org/10.1051/lhb/2020055, 2020.

Pontes, P. R. M., Fan, F. M., Fleischmann, A. S., de Paiva, R. C. D., Buarque, D. C., Siqueira, V. A., Jardim, P. F., Sorribas, M. V., and Collischonn, W.: MGB-IPH model for hydrological and hydraulic simulation of large floodplain river systems coupled with open source GIS, Environmental Modelling & Software, 94, 1–20, https://doi.org/10.1016/j.envsoft.2017.03.029, 2017.

Pujol, L., Garambois, P.-A., and Monnier, J.: Multi-dimensional hydrological–hydraulic model with variational data assimilation for river networks and floodplains, Geoscientific Model Development, 15, 6085–6113, https://doi.org/10.5194/gmd-15-6085-2022, 2022.

Quintana-Seguí, P., Moigne, P. L., Durand, Y., Martin, E., Habets, F., Baillon, M., Canellas, C., Franchisteguy, L., and Morel, S.: Analysis of Near-Surface Atmospheric Variables: Validation of the SAFRAN Analysis over France, Journal of Applied Meteorology and Climatology, 47, 92–107, https://doi.org/10.1175/2007jamc1636.1, 2008.

Sandre: Document de présentation - DESCRIPTION DU REFERENTIEL HYDROGRAPHIQUE (BD TOPAGE®), Tech. rep., OFB, IGN, ST SANDRE, 2020.

Shrestha, P. K., Samaniego, L., Rakovec, O., Kumar, R., and Thober, S.: A Novel Stream Network Upscaling Scheme for Accurate Local Streamflow Simulations in Gridded Global Hydrological Models, Water Resources Research, 61, e2024WR038 183, https://doi.org/https://doi.org/10.1029/2024WR038183, 2025.

Sood, A. and Smakhtin, V.: Global hydrological models: a review, Hydrological Sciences Journal, 60, 549–565, https://doi.org/10.1080/02626667.2014.950580, 2015.

Sousa, T. M. I. and Paz, A. R.: How to evaluate the quality of coarse-resolution DEM-derived drainage networks, Hydrological Processes, 31, 3379–3395, https://doi.org/10.1002/hyp.11262, 2017.

https://doi.org/10.5194/egusphere-2026-1557
Preprint. Discussion started: 27 March 2026

Towner, J., Cloke, H. L., Zsoter, E., Flamig, Z., Hoch, J. M., Bazo, J., Coughlan de Perez, E., and Stephens, E. M.: Assessing the performance of global hydrological models for capturing peak river flows in the Amazon basin, Hydrology and Earth System Sciences, 23, 3057–3080, https://doi.org/10.5194/hess-23-3057-2019, 2019.

Vidal, J.-P., Martin, E., Franchistéguy, L., Baillon, M., and Soubeyroux, J.-M.: A 50-year high-resolution atmospheric reanalysis over France with the Safran system, International Journal of Climatology, 30, 1627–1644, https://doi.org/https://doi.org/10.1002/joc.2003, 2010.

Vogt, J. V., Colombo, R., and Bertolo, F.: Deriving drainage networks and catchment boundaries: a new methodology combining digital elevation data and environmental characteristics, Geomorphology, 53, 281–298, https://doi.org/10.1016/s0169-555x(02)00319-7, 2003.

Wang, L. and Liu, H.: An efficient method for identifying and filling surface depressions in digital elevation models for hydrologic analysis and modelling, International Journal of Geographical Information Science, 20, 193–213, https://doi.org/10.1080/13658810500433453, 2006.

Wang, Y.-J., Qin, C.-Z., and Zhu, A.-X.: Review on algorithms of dealing with depressions in grid DEM, Annals of GIS, 25, 83–97, https://doi.org/10.1080/19475683.2019.1604571, 2019.

Yamazaki, D., Oki, T., and Kanae, S.: Deriving a global river network map and its sub-grid topographic characteristics from a fine-resolution flow direction map, Hydrology and Earth System Sciences, 13, 2241–2251, https://doi.org/10.5194/hess-13-2241-2009, 2009.

Yamazaki, D., Baugh, C. A., Bates, P. D., Kanae, S., Alsdorf, D. E., and Oki, T.: Adjustment of a spaceborne DEM for use in floodplain hydrodynamic modeling, Journal of Hydrology, 436-437, 81–91, https://doi.org/https://doi.org/10.1016/j.jhydrol.2012.02.045, 2012.

Yamazaki, D., de Almeida, G. A. M., and Bates, P. D.: Improving computational efficiency in global river models by implementing the local inertial flow equation and a vector-based river network map, Water Resources Research, 49, 7221–7235, https://doi.org/10.1002/wrcr.20552, 2013.

Yamazaki, D., Ikeshima, D., Tawatari, R., Yamaguchi, T., O'Loughlin, F., Neal, J. C., Sampson, C. C., Kanae, S., and Bates, P. D.: A high-accuracy map of global terrain elevations, Geophysical Research Letters, 44, 5844–5853, https://doi.org/10.1002/2017gl072874, 2017.

Yamazaki, D., Ikeshima, D., Sosa, J., Bates, P. D., Allen, G. H., and Pavelsky, T. M.: MERIT Hydro: A High-Resolution Global Hydrography Map Based on Latest Topography Dataset, Water Resources Research, 55, 5053–5073, https://doi.org/10.1029/2019wr024873, 2019.

Zhang, J., Lian, Y., Duan, Q., Liu, Z., Mao, X., Ling, M., and Guan, Y.: Coupled hydrologic and hydraulic modeling for a lowland river basin in China, Journal of Hydrology, 649, 132 470, https://doi.org/10.1016/j.jhydrol.2024.132470, 2025.